JCTC Journal of Chemical Theory and Computation

Article

pubs.acs.org/JCTC

Quantum Chemical Benchmark Study on 46 RNA Backbone Families Using a Dinucleotide Unit

Holger Kruse,*[,†,‡] Arnost Mladek,[†] Konstantinos Gkionis,[†,‡] Andreas Hansen,[§] Stefan Grimme,*[,§] and Jiri Sponer*[,†,‡]

[†]Institute of Biophysics, Academy of Sciences of the Czech Republic, Královopolská 135, 612 65 Brno, Czech Republic

[‡]CEITEC—Central European Institute of Technology, Campus Bohunice, Kamenice 5, 625 00 Brno, Czech Republic

[§]Mulliken Center for Theoretical Chemistry, Institut für Physikalische und Theoretische Chemie der Universität Bonn, Beringstr. 4, D-53115 Bonn, Germany

Supporting Information

ABSTRACT: We have created a benchmark set of quantum chemical structure−energy data denoted as UpU46, which consists of 46 uracil dinucleotides (UpU), representing all known 46 RNA backbone conformational families. Penalty-function-based restrained optimizations with COSMO TPSS-D3/def2-TZVP ensure a balance between keeping the target conformation and geometry relaxation. The backbone geometries are close to the clustering-means of their respective RNA bioinformatics family classification. High-level wave function methods (DLPNO−CCSD(T) as reference) and a wide-range of dispersion-corrected or inclusive DFT methods (DFT-D3, VV10, LC-BOP-LRD, M06-2X, M11, and more) are used to evaluate the conformational energies. The results are compared to the Amber RNA bsc0χ_{OL3} force field. Most dispersion-corrected DFT methods surpass the Amber force field significantly in accuracy and yield mean absolute deviations (MADs) for relative conformational energies of ∼0.4−0.6 kcal/mol. Double-hybrid density functionals represent the most accurate class of density functionals. Low-cost quantum chemical methods such as PM6-D3H+, HF-3c, DFTB3-D3, as well as small basis set calculations corrected for basis set superposition errors (BSSEs) by the gCP procedure are also tested. Unfortunately, the presently available low-cost methods are struggling to describe the UpU conformational energies with satisfactory accuracy. The UpU46 benchmark is an ideal test for benchmarking and development of fast methods to describe nucleic acids, including force fields.

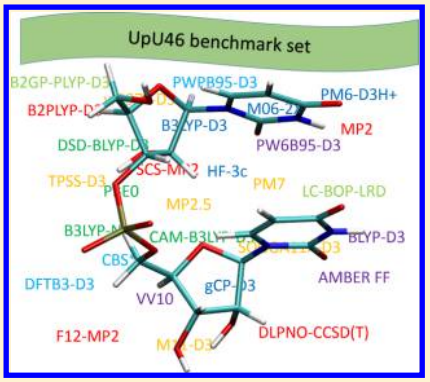

INTRODUCTION

RNA is accountable for a wide pool of functions in biology, and more and more of its functions are still being discovered. While only ∼2% of the genomic DNA directly encodes proteins, 80% or more or the genome is transcribed into RNA. Therefore, large part of the DNA genome is coding nonprotein coding RNAs.[1] The typical RNA macromolecule is a single-stranded, polynucleotide (A, C, G, and U nucleotide units) chain that possesses a high likelihood to fold back on itself to form a complex tertiary (three-dimensional, 3D) structure.[2] The presence of the 2′-hydroxyl (2′−OH) group attached to the C2′ atom of the sugar unit enables the formation of a tremendous array of astonishingly variable and highly complex structures.[3] Folded RNA regions consist of short Watson−Crick double helices that alternate with non-Watson−Crick regions.[4] The non-Watson−Crick RNA regions, although formally unpaired at the secondary (2D) structure level, usually fold into precisely shaped tertiary 3D structures, where every single hydrogen bond, stacking arrangement, or local backbone conformation matters.[4b,5] This complicates RNA structure predictions from the sequence[2,6] as well as molecular modeling, quantum chemistry, atomistic simulations and other computational chemistry approaches.[7,4b,8,9]

It is well-established that approximations of classical pair-additive force fields (FFs) that dominate contemporary modeling of nucleic acids may sometimes lead to considerable artifacts in large-scale simulation studies.[10]

The so-called "RNA motifs" are recurrent, robustly 3D-shaped RNA building blocks that are defined through ordered arrays of noncanonical and canonical base pair interactions, complemented by distinct consecutive local backbone conformations.[4b,11] An RNA backbone geometry classification is a useful framework for discussing the finer points of RNA backbone structures. Recent studies formulating RNA backbone geometry classification often use *suites* rather than nucleotides as the basic conformational unit,[5b] as reviewed elsewhere.[10b] A suite is a sugar-to-sugar backbone segment including the seven consecutive backbone dihedrals between the δ_i and δ_{i+1} backbone angles of two consecutive nucleotides numbered i and $i + 1$ (cf. Figure 1). A total of 46 different suite

Received: June 2, 2015
Published: September 2, 2015

DOI: 10.1021/acs.jctc.5b00515
J. Chem. Theory Comput. 2015, 11, 4972−4991

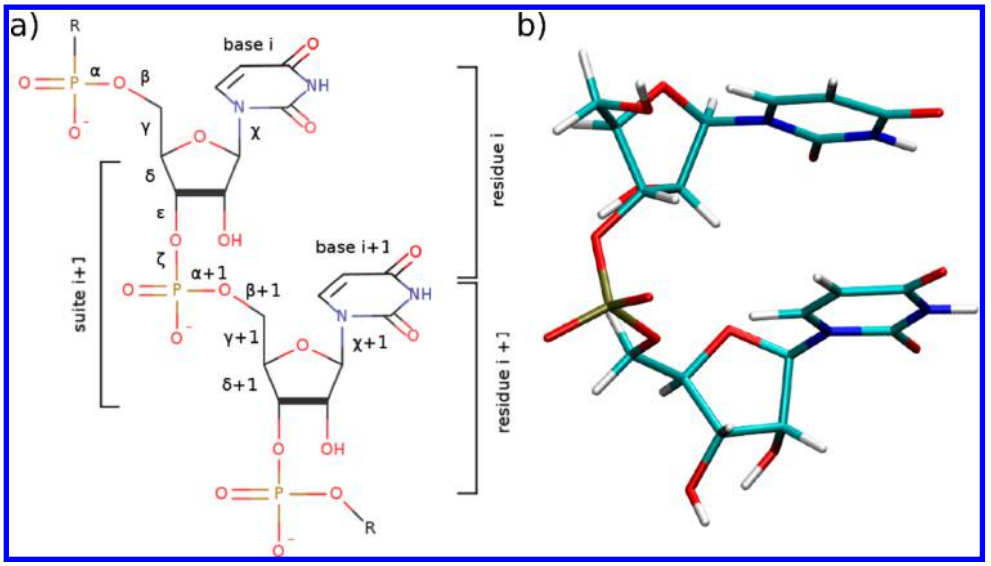

Figure 1. (a) Naming scheme of the backbone topology and (b) depiction of the actual UpU dinucleotide model (conformation **1a**). Consecutive sugar−phosphate backbone segments can be defined using two possible ways. The residue (e.g., the nucleotide unit) is defined from phosphate to phosphate and includes six torsional angles (α to ζ) and the glycosidic torsion angle χ. The conformation of the suite excludes the χ angles and ranges from δ_i to δ_{i+1}. The suite is numbered according to the i+1 nucleotide. The suite-based description[5b] of the sugar−phosphate backbone is used in this paper.

conformations (conformational substates, distinct combinations of the backbone dihedrals) have been suggested as a consensus set of dominantly occurring backbone conformations in known RNA structures.[5b] These distinct RNA backbone rotamers enable the formation of diverse RNA topologies.

In the present study, we provide quantum chemical (QM) benchmark calculations on the relative energies of the consensus set of 46 RNA backbone families, using an UpU dinucleotide step as the model system. Our benchmark database thus contains 46 UpU geometries and their relative electronic structure energies calculated by high-accuracy QM methods. The purpose of such benchmark databases is to collect a set of representative structure−energy points on accurate potential energy surfaces of the studied systems. The benchmark data can then be used for verification and parametrization of other computational methods. Benchmark databases have played an instrumental role in recent developments of many computational chemistry methods.[12] UpU is the largest nucleic acid model system so far considered for QM benchmark purposes. Our model system includes, for the first time, simultaneously three important energy contributions, namely, the backbone conformation, the base stacking and the base-backbone coupling. We show that the accurate inclusion of these three energy contributions possesses a considerable challenge for faster computational methods.

An essential methodological advancement to create the UpU46 database is the use of restrained optimizations.[13] In order to create the structure−energy database, we first need to obtain a set of high-quality geometries corresponding to the target structures of the RNA backbone families, i.e., to the combinations of the backbone dihedral angles that exist in experimental structures.[5b,10b,13] At the same time, the geometries should be sufficiently relaxed, so that their electronic structures are not frustrated. The restrained optimization[13] targeting the experimentally known RNA backbone families is, in our opinion, the only viable approach to derive such geometries. Unprocessed geometries directly taken from the experimental structures cannot be used for energy calculations. Unconstrained optimization cannot be applied, because even when using the continuum solvent environment, many target structures would be lost, i.e., the optimizations would radically change the backbone dihedrals. Furthermore, while providing basic screening of the long-range electrostatics, the mean-field continuum solvent does not fully mimic a real atomistic solvent environment. The optimized structures are often spoiled by gas-phase-like structural artifacts, since the continuum solvent is insufficient to prevent the formation of non-native intramolecular hydrogen bonds and other undesired structural features. This issue is discussed in more detail elsewhere.[13,14] Conventional constrained QM optimizations are also unsuitable, because of the genuine error margins inherent to the RNA structures obtained by structural bioinformatics that may be associated with structural conflicts between the individual dihedral angles.[5b,10b,13] Such conflicts remain uncorrected upon constrained optimizations. They would bias the calculated energies and cause distortions of the unconstrained parameters. Unconstrained and tightly constrained optimizations were both shown to be inadequate, even for smaller nucleic acid backbone fragments.[15] Thus, to the best of our knowledge, restrained optimizations[13] represent the best option to reliably derive sufficiently relaxed structures of RNA model systems that do not deviate from the target conformations. Appropriately chosen harmonic restraints provide the necessary flexibility of a few degrees for the individual dihedrals to resolve the structural conflicts while keeping the structures within the target backbone families, and are close to the centroid structures derived by structural bioinformatics.[5b] Except for the relaxation of bond lengths and valence angles, the QM-optimized and bioinformatics structures are then essentially identical. The biochemical relevance of our work stems from the fact that the studied structures include all known RNA backbone families that have been identified by structural bioinformatics studies, as in detail explained in the literature.[5b,10b] All structures obtained by the restrained QM optimizations remain very similar to the reference bioinfor-

DOI: 10.1021/acs.jctc.5b00515
J. Chem. Theory Comput. 2015, 11, 4972−4991

matics structures, as quantified by the suiteness analysis given below.[5b]

Noncovalent interactions (NCI) play a fundamental role in many areas of chemistry, physics, and biology. Their crucial role in the stability of RNA and DNA biomolecules is known for decades.[16] NCI have been a focus of numerous benchmark QM studies. The London dispersion energy, which often is considered to be weak, can in fact account for a large percentage of the interaction energy of isolated molecular complexes, surpassing contributions from classical electrostatics and hydrogen bonding.[17] However, the (free) energy balance in full biopolymers is much more complex. In fact, the exact balance between free-energy contributions from dispersion and classical electrostatics, or between stacking and hydrogen-bonding interactions in nucleic acids is unknown. The relative contributions of different energy terms to the final free-energy balances are notoriously difficult to extract from the experiments, and the outcomes of the measurements are dependent on the structural context (the type of nucleic acid architecture), its environment, and the free-energy reference state used.[18] In fact, a specific interaction, such as base stacking or hydrogen bonding, can even have an opposite effect on the stability when embedded in different types of nucleic acid structures, demonstrating the very weak correlation between the intrinsic energetics (potential energies) of different contributions and the final free energies.[18] Therefore, it is very useful to complement the experiments by advanced computational methods. The calculations should be done on systems that are as complete as possible and care should be taken with regard to the sampling of the conformational space.[19] In principle, full-scale free-energy computations could allow one to better separate the roles of different energy contributions, compared to experiments. Unfortunately, the accuracy of free-energy computations is a common problem and the free-energy decompositions are especially challenging.[19c,d,20] Rigorously, free-energy evaluation requires a robust Boltzmann sampling of the statistical ensemble, something that is often not achievable, even using the fastest atomistic MM level of description.[21] Nevertheless, accurate QM computations can, e.g., help to refine free-energy estimates obtained by MM-based simulation approaches, effectively combining the sampling and explicit solvation effects provided by an MM simulation method, and the more physical description of the intrinsic energetics by a QM method.[14a] Thus, there is a high demand for the development of fast, but sufficiently accurate, QM methods to study nucleic acids.

An important requirement to compute structures and energies of nucleic acids is the accurate treatment of long-range correlation effects such as the London dispersion interactions. Sometimes dispersion interactions are imprecisely called van der Waals interactions. With dispersion interactions, we are roughly referring to the attractive part of the van der Waals potential that is commonly used in the biomolecular modeling field. Recent years showed immense progress in treating dispersion interactions within the framework of density functional theory (DFT),[22] opening a path for much more reliable QM computations on nucleic acids. However, an often less-appreciated fact, at least in the QM literature, is that the intrinsic conformational preferences of the sugar phosphate backbone, and their interplay with base stacking and hydrogen bonding interactions, are at least equally important to describe the structural dynamics and stability of nucleic acids. QM studies including the nucleic acids backbone[10b,15,23] are much less frequent than studies of base−base interactions.[18,24] In fact, contemporary pair-additive biomolecular force fields and probably many other fast computational methods have much larger problems to accurately describe the potential energy surface (PES) of the sugar−phosphate backbone than the common NCI such as base stacking.[10a,b,25] Balanced computational methods should be capable to describe both NCI and the sugar−phosphate backbone simultaneously, suggesting that a dinucleotide is a vital test system.

Wave function methods offer a more systematic approach to calculate correlation energy than DFT, but they share their own set of difficulties. Two major drawbacks are (i) higher one-particle (atomic orbital) basis set demands, slower basis set convergency, and (ii) overall higher computational cost. It was shown that dispersion-corrected DFT often surpasses low-order wave-function-based correlation methods such as MP2 and SCS-MP2, even in their basis set limit.[24j,26] The high computational cost of the "gold standard" level CCSD(T) calculations often prohibits calculation of even moderately sized molecules (>30 atoms). For the dinucleotide system, we found that CCSD(T) calculations with a sufficiently large basis set are not yet routinely tractable. Thus, we had to search for alternative options that, although being somewhat less rigorous than CCSD(T), would still allow us to execute sufficiently reliable calculations on RNA dinucleotides routinely. Note that, in the near future, we plan to extend the study to other sequences and to investigate the multidimensional conformational space of the RNA backbone families in more detail, which will require the assessment of thousands of dinucleotide structures. Since our main goal is to provide benchmark datasets for fast QM methods applicable for large fragments of nucleic acids, we can tolerate a somewhat less rigorous level of the reference QM calculations than the CCSD(T) level.

Advances in local orbital approximations led to the recent formulation of the domain-based, local pair-natural orbital approximation (DLPNO)[27] approach that enables routine CCSD(T) calculations of over 100 atoms with triple-ζ atom orbital (AO) basis sets. Unlike other local CCSD(T) quality formulations, the objective of the DLPNO technique is to reproduce the canonical coupled-cluster (CC) results. Experience with DLPNO−CCSD(T) is still somewhat limited, and recent benchmark studies (e.g., on transition-metal reactions[28] or large organic molecules[29]) explore the advantages and limitations of the method. Neese et al. recently studied the accuracy limits of DLPNO in greater detail and suggested tighter parameter thresholds for systems in which NCI are the dominant interaction energy component.[30] In our study, we finally decided to use a new computational protocol abbreviated as DLPNO−CCSD(T)/CBS*, which combines DLPNO−CCSD(T) with a new multiplicative complete basis set (CBS) extrapolation scheme (denoted as CBS*), as the reference method. The protocol has been proposed by some of the present authors, and its full derivation and testing for general systems will be published separately.[29] Nevertheless, the Computational Details section of the present paper includes all of the technical details that are necessary to execute the computations.

Benchmark level conformational energies of the RNA sugar−phosphate backbone have earlier been calculated using a minimalistic RNA backbone model consisting only of the sugar−phosphate-sugar (rSPS) backbone unit.[31] Herein, we investigate a complete dinucleotide by adding uracils to the rSPS model and then carefully refining the geometries. This is a

DOI: 10.1021/acs.jctc.5b00515
J. Chem. Theory Comput. 2015, 11, 4972−4991

very fundamental extension of the model system. Using these benchmark geometries, we test different types of dispersion corrections for DFT, which is the main workhorse for large biochemical molecules. A detailed overview and classification of different approaches can be found elsewhere.[22] The DFT-D3 approach is a semiclassical C_n-based method applying an atom pairwise sum over potentials of the form $-C_n/R^n$, with $n = 6$ and 8 and C_n being the nth-order dispersion coefficient for an atom pair. The $n = 6$ potential is the dominant contributor to the dispersion energy. This approach provides the correct R^{-6} asymptotic decay of the dispersion interaction at a negligible computation cost, but it neither explicitly modifies nor depends on the electron density. However, geometry-dependent information modifies the applied C_6 coefficients through a fractional coordination number approach. A related approach is the local-response dispersion (LRD) method by Sato et al.[32] used in the LC-BOP-LRD functional herein, which obtains the C_6 coefficient directly from the electron density. The vdW-DF method[33] computes the dispersion interaction of a system solely from its electron density. A so-called nonlocal (NL) correlation (dispersion) energy term is added to conventional DFT energy similar to DFT-D3. We apply the VV10 functional and its extension to other xc-kernels, which is dubbed DFT-NL.[34] Although the NL correction can be applied self-consistently and thus can modify the electron density, it is typically applied in a computationally less-expensive post-SCF fashion without a significant loss in accuracy. In structure and energy benchmark studies, the penalty of the non-SCF treatment was insignificant.[35] We also test four density functionals developed in the Truhlar group (M06-2X, M11, M11-L, and SOGGA11X), which capture medium-range dispersion interactions through a highly parametrized exchange-correlation potential.[36] Their drawback is an increased numerical sensibility toward the quadrature grid,[37] as well as a too fast asymptotic decay of the dispersion interactions, leading to under-binding effects at long-range distances.[24k] It was shown that M06 and M06-2X could benefit from adding a D3(0)-correction to account for the missing long-range dispersion interaction.[24k,26] In addition, wave function methods such as MP2, SCS-MP2,[38] and MP2-F12[39] are tested. Furthermore, we also test low-scaling semiempirical QM methods like PM6[40] and its variants, DFTB3-D3,[41] HF-3c,[42] and others. These methods are already fast enough to offer improved sampling in QM studies of nucleic acids. The results will be put into perspective with data obtained using the Amber bsc0χ_{ol3}[43] FF variant of the Cornell et al.[43a] force field, which is one of the recently suggested reparametrizations of the RNA force field and is presently widely used. In addition, a few basic hybrid mechanical/molecular mechanical (QM/MM) computations are tested.

COMPUTATIONAL DETAILS

Software. The following program packages were utilized: ORCA V.3.0.2 and V.3.0.3,[44] Gaussian 09,[45] Gamess,[46] Mopac12,[47] Amber12,[48] dftb+,[49] and Turbomole V.6.3.[50]

Gaussian09 was employed for the M11-L,[51] M11,[52] SOGGA11-X,[53] M06-2X,[36] and ONIOM[54] calculations. The def2-QZVP and def2-TZVP[55] basis sets were taken from the EMSL.[56]

The QM/MM calculations were performed using the ONIOM method. Two different partitioning schemes were applied: (a) nucleobases were placed within the high-level layer (QM) and the sugar−phosphate backbone within the low-level layer (MM) and (b) *vice versa*. Hydrogen link atoms were used in all cases to account for the breaking of the sugar-base bond at the layer boundary. Specifically, hydrogen link atoms replaced the sugar carbon atoms of the C1′-N1 bond in partitioning scheme a and the base nitrogen atoms of the C1′−N1 bond in partitioning scheme b. Note that replacing the C1′−N1 bond by C−H alters the polarity of the original bond, which may be a source of error. In both cases, the link atoms were automatically positioned along the vector of the original C1′−N1 bond using the default parameters of the software. All calculations were performed with and without electrostatic embedding (EE). TPSS[57]-D3/def2-TZVP was applied for the QM layer, and the MM layer was described by the bsc0 variant of the Amber FF.

Gamess was employed for the LC-BOP-LRD[32] calculations, using a tightened integral screening threshold of 1×10^{-11} E_h and a (99/434) quadrature grid.[58] The def2-QZVP basis set was taken again from the EMSL.

Mopac12 was employed for PM6 and PM7[59] methods with tightened SCF convergence using the *PRECISE* keyword.

dftb+ was employed for the DFTB3 calculations. The D3H +[60] correction for PM6 was implemented in our dftd3[61] code. The code for the 'H+' hydrogen bond correction itself was taken from github.[60]

The **Amber12** suite was employed for the Cornell et al. Amber FF[43a] with the bsc0[43c] and χ_{OL3}[43b] corrections. A review of nucleic acid AMBER force fields was recently published.[10a]

Turbomole was used for all COSMO TPSS-D3(BJ)/def2-TZVP structure optimizations combined with the external optimizer program *xopt*.[13]

ORCA Calculations. The remaining methods were calculated using ORCA. Where applicable, the resolution of identity (RI, density fitting) approximation to the Coulomb integrals and the chain of sphere approximation COSX[62] to the exchange integrals were employed. All wave function methods used the frozen-core approximation. The SCF was converged to at least 10^{-7} E_h, using the *TightSCF* keyword. Nondefault integration grids were used: *grid5* for the xc-potential and *gridx5* for the COSX integration. The gCP correction[63] was applied using the ORCA implementation. The nonlocal NL correction[34] based on VV10[33] was applied as a post-SCF correction. The DLPNO−CCSD(T)[27] calculation applied a tightened threshold for the $T_{CutPairs}$ parameter of 10^{-5} E_h. RI-MP3/def2-SVPD[64] calculations were performed for MP2.5/ΔCBS. The RI-MP2-F12 calculations used the cc-pVDZ-F12 and corresponding cc-pVDZ-F12-CABS basis sets, and the cc-pVTZ auxiliary basis set[65] for the density fitting. COSMO[66] calculations used the default values implemented in ORCA for water as a solvent. DFT calculations with COSMO employed the numerical integration of the COSMO potential.

The atom-pairwise D3 dispersion correction[61] was applied using both the zero-damping function denoted as D3(0) and the default Becke−Johnson damping[67] function denoted as D3(BJ). Most functionals were applied with D3(BJ). Methods that already include dispersion interaction in the medium-range region by their functional form, e.g. M06-2X and M11, or parametrization, such as PM6, often combine better with the D3(0) version. The D3(0) and D3(BJ) corrections were calculated using the dftd3 code.[61]

The Suitename program[68] was used to calculate the suiteness values and backbone classifications. Molecular structures were visualized using VMD.[69]

DFT−D3 Parameters for M11-L, M11, and SOGGA11X. The M11-L, M11, and SOGGA11X functionals are newer DFs

DOI: 10.1021/acs.jctc.5b00515
J. Chem. Theory Comput. 2015, 11, 4972−4991

Table 1. Overview of the Backbone Angles of the UpU Dinucleotides Benchmark Set Geometries

	Angles (deg)										
family[a]	δ	ε	ζ	$\alpha+1$	$\beta+1$	$\gamma+1$	$\delta+1$	χ	$\chi+1$	$\delta\delta\gamma$[b]	suiteness
1a	82	211	287	293	175	55	83	196	205	33p	0.982
1m	85	218	292	292	223	58	88	206	258	33p	0.985
1L	87	245	268	303	140	61	81	224	191	33p	0.991
&a	81	190	265	295	181	52	84	204	204	33p	0.983
7a	84	217	222	303	161	50	84	191	185	33p	0.995
3a	86	215	172	289	165	47	86	205	227	33p	0.993
9a	84	210	120	288	155	49	84	206	182	33p	0.977
1g	83	218	290	166	159	50	86	195	200	33p	0.987
7d	86	238	256	70	170	53	86	235	186	33p	0.988
3d	86	244	204	66	181	54	86	190	193	33p	0.998
5d	82	202	63	67	142	49	85	191	181	33p	0.978
1e	81	201	281	250	82	169	86	196	182	33t	0.997
1c	82	194	289	154	194	180	86	205	192	33t	0.969
1f	82	200	292	171	139	176	86	200	186	33t	0.990
5j	88	224	80	67	108	176	84	205	192	33t	0.998
1b	86	216	287	299	179	59	146	190	239	32p	0.983
1[	84	228	293	292	221	54	148	198	283	32p	0.912
3b	85	225	167	292	178	49	148	202	218	32p	0.996
1z	84	208	277	194	162	49	146	201	241	32p	0.990
5z	84	207	55	164	149	50	148	210	216	32p	0.994
7p	85	237	219	68	200	53	147	220	235	32p	0.996
1t	81	195	286	178	195	175	149	203	215	32t	0.966
5q	84	209	70	65	119	177	148	207	51	32t	0.969
1o	85	217	287	296	225	294	152	237	308	32m	0.992
7r	86	233	247	63	181	295	151	205	59	32m	0.994
2a	145	262	289	287	193	53	85	225	189	23p	0.997
4a	147	259	168	296	170	51	85	222	187	23p	0.992
0a	150	221	140	285	157	47	85	252	193	23p	0.995
#a	149	193	148	288	150	42	86	255	189	23p	0.990
4g	149	256	165	203	164	48	84	245	185	23p	0.991
6g	144	262	79	205	190	59	88	225	267	23p	0.971
8d	149	271	242	63	176	54	88	246	181	23p	0.999
4d	151	251	188	80	199	60	88	271	195	23p	0.990
6d	147	242	89	60	161	52	84	204	193	23p	0.998
2h	148	263	290	295	177	177	87	239	195	23t	0.993
4n	149	274	99	82	247	183	84	274	210	23t	0.992
0i	149	275	99	81	247	182	85	234	191	23t	0.988
6n	151	268	83	63	191	177	87	231	65	23t	0.988
6j	143	244	65	72	121	181	84	221	200	23t	0.991
2[	147	260	291	292	211	55	149	238	252	22p	0.996
4b	147	244	163	294	172	46	147	248	228	22p	0.989
0b	148	247	111	274	164	55	147	236	226	22p	0.991
4p	148	261	213	72	207	56	148	77	226	22p	0.987
6p	147	258	89	68	172	55	149	231	247	22p	0.996
4s	150	248	169	278	85	177	148	217	265	22t	0.999
2o	148	257	296	288	194	294	151	227	245	22m	0.999

[a]Naming of the conformational families is according to the work by Richardson et al.,[5b] where all the bioinformatics details are given. [b]The $\delta\delta\gamma$ classification denotes the C2′ and C3′-endo sugar puckers according to the δ angles, and the *trans* (t), *gauche plus* (p), and *gauche minus* (m) regions of the angle γ, as further explained in the text.

from Truhlar's group incorporating improved xc kernels. Their application in benchmark studies focused on NCI have been limited so far, and D3 parameters have not yet been reported. The S66 benchmark set[24i] provides a comprehensive list of 66 different noncovalently bound molecular complexes and is a well-rounded test for noncovalent interactions. The S66 database mean absolute deviations (MADs) of the M11-L, M11, and SOGAA11X functional using the def2-TZVP basis set are 0.87, 0.34, 2.15 kcal/mol, respectively. We fitted the D3(0) correction using the fit set used in the original D3 publication.[61] Similar to the M06-2X-D3(0) fitting procedure,[24j] the s8 parameter in the D3(0) correction is set to zero to account for the inclusion of medium-range dispersion interactions in the functional form. The fitted values are presented in the Supporting Information. The D3(0) correction improves the S66 MAD of M11-L-D3(0) to 0.37 kcal/mol and the MAD of SOGGA11X-D3(0) to 0.44 kcal/

DOI: 10.1021/acs.jctc.5b00515
J. Chem. Theory Comput. 2015, 11, 4972−4991

mol. No improvement in the MAD is seen for M11-D3(0), since it remains at 0.34 kcal/mol.

Creation of the Database of Benchmark UpU Structures. Construction of appropriate geometries was a crucial step in this study. The UpU conformers have been prepared as follows. For each of the 46 RNA backbone conformational classes, a representative dinucleotide with values of the backbone torsion angles as close as possible to the average values ("clustering-mean") of a given family has been identified in experimental structures[5b] (see Table 1 in the work of Richardson et al.[5b] or Table S4 in the Supporting Information). This geometry is considered to be the best fitting geometry for each conformational family.[5b] Note that utilization of the representative structure is necessary to have a meaningful value of the χ angles, because they are not used for the classification. Subsequently, both the nucleobases of the representative dinucleotide have been manually replaced with uracils. The experimental glycosidic angles of the nucleobases have been preserved. All suite backbone torsions ($\delta - 1, ..., \delta$) have then been adjusted to the clustering-mean values of Richardson,[5b] as the representatives of each family are only close to, but do not match exactly, the clustering-mean of a given backbone family. The visual inspection of the manually constructed dinucleotides revealed no steric clashes or unnatural close contacts. To avoid double negative charges, the 5′ end phosphate groups of the UpU dinucleotides were replaced with hydroxyl groups. The UpU models are comprised of a full uridine nucleoside at the 5′ end connected through its O3′ via a phosphodiester linkage to a negatively charged nucleotide at the 3′ end (see Figure 1b).

Restrained optimizations[13] were performed using the COSMO-TPSS-D3(BJ)/def2-TZVP method with ε = 78.5 employing the open-source program xopt, together with Turbomole.[13] All backbone torsions from δ to δ + 1 and both glycosidic bond χ dihedrals were restrained with a restraining constant of 0.1 E_h/rad^2 at the aforementioned mean values from Richardson.[5b] The initial orientation of the 5′−OH group was set pointing away from the nucleobases, i.e., the H−O5′−C5′−C4′ angle is set to 180°, and left unrestrained except for the conformers **1[**, **1L**, **4p**, **7d**, and **1o**; see the work of Richardson et al.[5b] for the naming scheme. In these particular cases, an additional restraint of 0.1 E_h/rad^2 prevented spurious hydrogen-bonding between 5′−OH and the anionic phosphate group oxygen. The initial orientation of the 2′−OH group in the 5′-sugar moiety was set to a global minimum position, according to earlier work.[31] The initial orientation of both the 3′-sugar hydroxyl groups was chosen as such that the 2′−OH can potentially establish a hydrogen bond with the O3′ oxygen of the C2′-/C3′-endo sugars. Note that the 46 RNA families include all combinations of the ribose puckers (cf. Table 1). To ensure the planarity of all uracil bases, three additional dihedral restraints of 0.1 E_h/rad^2 per nucleobase were applied. Without this, the nucleobases would become nonplanar with extensive out-of-plane interactions that are not relevant for nucleic acids.[70] In the case of the **1g** and **2a** conformers, the base planarity was not a problem, since there was no stacking between the bases, and no planarity restraints were necessary. An example control file for the xopt program and all final geometries are available in the Supporting Information. Because of the rather tight restraints, the difference between the starting and optimized structures is insignificant and mostly below 3°. Table 1 lists all backbone dihedrals of the optimized UpU dinucleotides, along with Richardson's suiteness classification, and Figure 2 showcases the structural variability with six structures. The suiteness parameter reports the conformer

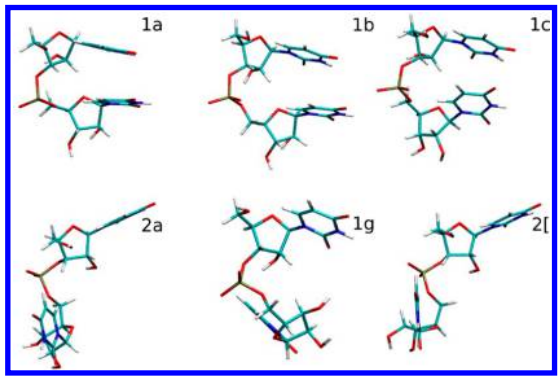

Figure 2. Depiction of six backbone families after restrained optimization with COSMO TPSS-D3/def2-TZVP, showcasing the variety of stacked (top row) and unstacked (bottom row) arrangements of the nucleobases.

match quality with respective to the clustering mean of a particular suite based on a scaled superellipsoid distance in the parameter space of all seven backbone angles.[5b] A suiteness value of 1.0 would indicate perfect agreement with the clustering-mean of a particular backbone family. All our structures give a value significantly above 0.9, with a vast majority of cases being above 0.98. This confirms that we generated a set of benchmark RNA QM structures balanced between ideal backbone family topology and relaxation by DFT-D3. The deviations of our QM-optimized structures from the representative bioinformatics standards[5b] are minimal and well below the error margins of the target structural data. The $\delta\delta\gamma$ classification[5b] denotes the sugar pucker for the (i − 1)th and ith nucleotide, where "2" stands for C2′-endo (δ = 120°−175°) and "3" stands for C3′-endo (δ = 55°−110°). The γ angle codes *t*, *p*, and *m* stand for *trans* (γ = 140°−215°), *gauche plus* (γ = 20°−95°), and *gauche minus* (γ = 260°−335°), respectively.

The unrestrained QM optimizations should, in no case, be used for biomolecular systems such as dinucleotides, as they would, in many cases, lead to a loss of the target conformation (cf. Table S5 in the Supporting Information). A common problem of unrestrained optimizations is the formation of non-native intramolecular interactions. Note that QM optimizations are more sensitive to these problems than MM optimizations, since the more physically correct QM description can overpower the continuum solvent relatively easily. As explained elsewhere, it does not indicate a better performance of the MM description, but it reflects mutual compensation of two errors: the lack of electronic structure rearrangements in the MM description and the absence of explicit interactions in the continuum solvent model.[13,14] In the Supporting Information, we demonstrate that unrestrained optimizations would often result into incorrect or very poor geometries. The optimization resulted either into a different family or into a nonclassifiable conformation in 9 of the 46 cases. Even those structures that remained in their respective families after the optimization did so with low suiteness values, e.g., the important **1a** structure yielded a suiteness value of only ∼0.3 without the restraints. It confirms that unrestrained QM optimizations of dinucleotides are essentially useless for any practical calculations.

DOI: 10.1021/acs.jctc.5b00515
J. Chem. Theory Comput. 2015, 11, 4972−4991

Selection and Justification of an Appropriate Computational Reference. The size of the system limits conventional CCSD(T) calculations to small double-ζ basis sets. Such calculations would be affected by nontolerable basis set errors. Furthermore, variable intramolecular basis set superposition errors are to be expected, due to variable degrees of stacking and orbital overlap in different structures. Even augmented double-ζ basis sets might be too small to guarantee accuracy that would be competitive with the best DFT-D3 functionals. Thus, we have searched for alternative options and employed the recently presented domain-based local pair natural orbital (DLPNO) ansatz for CCSD(T).[27] This particular local correlation method aims to recover the canonical CCSD(T) results as closely as possible, instead of primarily aiming for linear scaling efficiency.[30] One drawback of the DLPNO ansatz is the underlying semilocal MP2 foundation that is used to estimate the contributions from the neglected electron pairs, an issue shared by most local correlation methods. This limits accuracy of the method especially for the conformations with substantial base stacking. Conformations such as **5z**, **1L**, and even **1a** are prone to have an increased error from the DLPNO reference, as opposed to unstacked conformers such as **2h**. A rough estimate is that <10 families have a clear stacking arrangement where MP2 becomes problematic, meaning that DLPNO should be reliable enough for a statistical evaluation, even though the error margin might be larger for specific conformations. A more-detailed look at these issues is planned for the future.

After considering several options, we employ the multiplicative complete basis set protocol marked as CBS*, as proposed by Hansen et al.,[29] which is composed as follows:

$$E^{\mathrm{CBS*}}_{\mathrm{DLPNO\text{-}CCSD(T)}} = E^{\mathrm{CBS(2,3)}}_{\mathrm{SCF}} + \left(\frac{Ec^{\mathrm{TZ}}_{\mathrm{DLPNO\text{-}CC}}}{Ec^{\mathrm{TZ}}_{\mathrm{MP2}}}\right) \times (f_{\mathrm{d}} \times Ec^{\mathrm{CBS(2,3)}}_{\mathrm{MP2}}) \quad (1)$$

The formation of the quotient of the DLPNO and the MP2 correlation energy weakens the influence that the MP2/CBS calculation has on the final result. The factor $f_{\mathrm{d}} = 1.08$ accounts for missing contributions from diffuse functions, following observations made by Hesselmann et al.,[71] and TZ refers to the def2-TZVP basis set.

The accuracy of the DLPNO approximation can be improved with a reasonable increase of computational cost by adjusting the cutoff threshold for the estimated pair correlation energies (T_{CutPairs} keyword) to 10^{-5} E_{h}.[28] A later study suggests using "TightPNO", which denotes a set of thresholds for noncovalent interactions,[30] which also includes $T_{\mathrm{CutPairs}} = 10^{-5}$, but tightens two additional cutoffs. The additional cutoffs have only a minor impact, compared to the key T_{CutPairs} quantity. The CBS* protocol suggests to change only T_{CutPairs}, which we followed in this work. For the **1a** conformation, this leads to about twice the amount of electron pairs kept for the calculations, compared to the less conservative default threshold of 10^{-4} E_{h}. The calculation still finishes within ∼1 day on a Xeon E5-2670 multicore node. It is important to note that the DLPNO−CCSD(T) method can be applied to even larger model systems such as GpG, or for systematic scans of the conformational space, which we plan to consider in future studies.

As a word of caution, we point out that there is still a lack of experience with DLPNO reference calculations for larger systems, especially since no conventional CCSD(T) data with large basis set are available for comparison. We use the DLPNO−CCSD(T)/CBS* scheme as our reference method. However, because of a remaining uncertainty regarding the actual error margin, one should consider the DLPNO−CCSD(T)/CBS* scheme as a high level wave function method and the best used herein, instead of being an "ultimate quality reference" commonly available for small molecule benchmarks. The decision between canonical and DLPNO−CCSD(T) calculations comes also down to choosing between a canonical CCSD(T)/double-ζ calculation with a notable basis set error and a DLPNO−CCSD(T)/triple-ζ calculation that neglects certain electron-pair correlation energy contributions, but applies a much more suitable basis set. We assume that the resulting overall error of the DLPNO approximation is smaller than the general basis set error, e.g., def2-SVP versus def2-TZVP. This is supported by the recent study of Liakos et al.,[30] which showed that the error due to the DLPNO approximation for common noncovalent interactions is well below 0.5 kcal/mol, relative to CCSD(T), at least with tighter cutoff values. Hence, the uncertainty of our DLPNO−CCSD(T)/CBS* reference can be mainly attributed to the basis set issues.

Note that the BSSE in the UpU conformers is formally intramolecular and is neither easily correctable nor unambiguously defined. We cannot apply the counterpoise correction commonly used for interaction energies. Nevertheless, the remaining BSSE after proper CBS extrapolation can be assumed to be small. This is another reason justifying our choice of the reference method that is further supported by the excellent performance of the DLPNO−CCSD(T)/CBS* scheme for association energies of large supramolecular complexes with up to 200 atoms and 5000 basis functions, reaching an MAD of ∼1 kcal/mol, relative to experimental values.[29] Hence, the DLPNO−CCSD(T)/CBS* method should be well-suited for future investigations of even larger nucleic acid building blocks.

Another challenge in our system is the anionic charge, which usually requires diffuse basis functions. The CBS* protocol corrects for missing diffuse functions by using the scaling factor of 1.08, but does not offer the spatial freedom needed for the correct physical description of the net negative charge. However, the def2-TZVP basis set contains at least semidiffuse basis functions that partly cover the physical requirement. Future studies are needed to elucidate the exact basis set dependencies. A further complication arises from the comparison of stacked and unstacked conformations, for which the error compensation effects may be less efficient. We also include a note on the problematic application of DFT for anionic systems further below.

As explained above, because of the size of the system, our reference calculations are affected by larger uncertainties than those common for smaller systems. However, the double-hybrid density functional (DHDF) calculations can be used as an independent secondary quality check, since they have been benchmarked numerous times[24k,72] using a wide array of different systems and have been proven to be very robust with high accuracy. We obtain a very good agreement between DHDF data and the suggested DLPNO−CCSD(T)/CBS* reference, as we extensively discuss below. Based on mutual consistency between the DLPNO−CCSD(T)/CBS* and DHDF data, we propose that both datasets can be safely used as benchmarks for low-cost methods, having errors that are typically an order of magnitude larger.

For the CBS extrapolation itself, the HF energy and the MP2 correlation energy are separately extrapolated using the

DOI: 10.1021/acs.jctc.5b00515
J. Chem. Theory Comput. 2015, 11, 4972−4991

Table 2. DLPNO−CCSD(T)/CBS* Gas-Phase Conformational Energies for the UpU46 Benchmark Set and Their Comparison with Other Selected Methods

	Energies (kcal/mol)							
conformation	reference[a]	PWPB95-D3(BJ)	PW6B95-D3(BJ)	TPSS-D3(BJ)	AMBER FF[b]	M06-2X-D3(0)	SCS-MP2/CBS(3,4)	M06-2X
1a	4.87	5.5	5.8	5.4	6.8	5.6	5.6	6.5
1m	5.60	6.5	6.6	6.0	6.2	6.8	6.4	6.7
1L	3.25	3.1	3.1	3.5	3.4	2.6	4.0	3.7
&a	3.96	4.1	4.3	4.9	5.0	3.5	4.4	4.0
7a	7.26	8.2	8.3	8.5	8.6	7.9	8.3	8.1
3a	6.84	7.4	7.6	6.7	5.8	7.5	6.8	7.4
9a	5.15	5.4	5.5	5.6	5.8	4.9	5.5	5.1
1g	2.22	2.8	2.9	2.7	3.8	2.0	2.9	2.5
7d	5.84	5.9	5.8	5.7	4.3	6.0	5.8	5.8
3d	5.42	5.7	5.8	5.7	5.6	5.3	5.2	5.0
5d	5.68	6.1	6.2	6.3	6.9	5.6	5.9	5.5
1e	11.13	12.3	12.5	11.8	14.9	11.5	11.9	11.6
1c	8.90	10.0	10.2	9.8	11.9	9.7	9.7	10.6
1f	14.41	14.2	14.2	14.0	17.7	13.6	13.7	13.9
5j	14.80	15.2	15.3	14.2	19.4	15.2	14.4	14.8
1b	2.97	3.6	3.6	3.9	3.8	3.9	4.2	4.9
1[	2.02	2.4	2.4	2.0	3.1	2.2	3.2	3.1
3b	6.09	6.5	6.6	6.2	6.6	6.5	6.2	6.5
1z	5.99	5.6	5.6	5.3	6.5	5.3	6.1	5.7
5z	0.57	0.0	−0.1	0.8	−1.6	−1.0	1.4	0.4
7p	3.90	3.7	3.6	3.4	5.4	4.0	3.7	3.8
1t	8.04	8.6	8.5	8.6	9.3	8.4	9.2	9.3
5q	12.48	13.1	13.2	12.1	16.4	12.6	12.8	12.6
1o	14.66	15.2	15.4	15.3	13.2	15.6	14.7	15.3
7r	13.98	14.1	14.2	13.9	15.7	14.3	13.7	14.2
2a	3.14	2.8	2.9	3.0	1.5	2.5	2.7	2.5
4a	6.34	6.3	6.4	6.5	5.6	5.8	5.7	5.7
0a	4.82	5.8	5.8	5.7	6.7	5.6	5.8	5.7
#a	4.92	5.4	5.6	4.8	6.0	5.2	5.5	5.5
4g	8.48	8.7	8.8	8.6	9.0	8.6	8.0	8.7
6g	8.03	9.2	9.4	8.5	5.3	9.7	9.0	10.4
8d	6.43	6.5	6.7	6.5	5.6	6.2	6.3	6.0
4d	6.82	7.4	7.5	7.0	7.7	7.0	6.8	6.9
6d	9.44	9.5	9.5	9.1	12.3	9.5	9.5	9.3
2h	10.42	10.8	11.1	10.8	11.6	10.7	10.2	10.2
4n	12.32	13.3	13.3	12.8	10.8	13.9	12.9	14.6
0i	6.74	6.8	6.7	6.9	6.4	7.1	7.2	7.8
6n	11.08	10.9	11.0	11.2	10.6	11.2	10.9	12.0
6j	16.61	16.6	16.6	15.7	21.2	16.6	15.8	16.2
2[	0.00	0.0	0.0	0.0	0.0	0.0	0.0	0.0
4b	5.48	5.7	5.7	5.5	4.5	5.8	5.6	6.0
0b	6.70	6.4	6.3	6.0	7.7	6.6	6.9	7.0
4p	10.24	10.1	10.2	9.9	14.0	10.7	10.0	10.6
6p	3.32	3.1	3.0	3.0	4.8	3.5	3.3	3.5
4s	18.20	19.0	19.2	18.0	20.8	19.2	18.3	19.1
2o	6.73	6.8	7.0	6.8	4.6	6.8	6.1	6.6

[a]Reference = DLPNO−CCSD(T)/CBS*. [b]The bsc0χ_{ol3} version

following two-point extrapolation schemes. The extrapolation scheme of Karton and Martin[73] is used for the HF energy:

$$E_{SCF}^{X} = E_{SCF}^{CBS} + A\exp(-\alpha\sqrt{X}) \quad (2)$$

where E_{SCF}^{X} is the SCF energy calculated with the basis set with cardinal number X and E_{SCF}^{CBS} is the SCF basis set limit energy. The constant A is to be determined as the unknown from the two resulting equations, and α is a basis set specific constant.

Following Halkier[74] and Truhlar,[75] the correlation energy can be extrapolated according to

$$E_{corr}^{CBS} = \frac{X^{\beta}E_{corr}^{(X)} - Y^{\beta}E_{corr}^{(Y)}}{X^{\beta} - Y^{\beta}} \quad (3)$$

where the β parameter is basis-set-specific. CBS(2,3) uses cc-pVDZ and cc-pVTZ basis set for the HF and MP2 extrapolation employing the optimized extrapolation coefficients of Neese and Valeev[76] (α = 4.420, β = 2.460). The CBS(3,4) extrapolation used for individual benchmarking of MP2 and SCS-MP2 uses def2-TZVPP and def2-QZVPP with α = 7.88 and β = 2.97.

DOI: 10.1021/acs.jctc.5b00515
J. Chem. Theory Comput. 2015, 11, 4972−4991

Table 3. Statistical Results from High-Level DFT Methods on the 46 UpU Conformers, Using the 2[Family as the Reference Point[a]

	MAPD (%)	MAD (kcal/mol)	MD (kcal/mol)	max/min dev (kcal/mol)	devR (kcal/mol)
B2PLYP-D3(BJ)	8.7	0.37	0.23	1.16/−0.79	1.95
B2GPPLYP-D3(BJ)	8.0	0.38	0.26	1.15/−0.49	1.63
PWPB95-D3(BJ)	9.0	0.43	0.30	1.22/−0.57	1.79
DSD-BLYP-D3(BJ)	8.6	0.33	0.15	0.99/−1.07	2.06
PW6B95-D3(BJ)	10.5	0.51	0.38	1.39/−0.63	2.20
B3LYP-D3(BJ)	12.0	0.52	0.40	1.45/−1.07	2.52
PBE0-D3(BJ)	8.4	0.43	0.30	1.45/−0.55	2.20
ωB97x-D3(0)	14.7	0.68	0.60	1.62/−1.19	2.81
CAM-B3LYP-D3(BJ)	13.2	0.71	0.63	1.64/−0.66	2.31
M06-2X	11.0	0.60	0.41	2.33/−0.64	2.97
M06-2X-D3(0)	13.1	0.47	0.21	1.71/−1.57	3.28
M11	15.1	0.92	0.81	3.08/−0.42	3.50
M11-D3	15.4	0.83	0.69	2.65/−0.94	3.59
SOGGA11X	57.9	1.83	1.36	6.38/−1.83	8.21
SOGGA11X-D3(0)	15.6	0.70	0.57	2.68/−1.14	3.82
B3LYP-NL	10.7	0.37	0.13	1.11/−1.52	2.63
LC-BOP-LRD	17.2	0.82	0.72	2.23/−1.68	3.91
BLYP-D3(BJ)	11.2	0.46	0.21	1.59/−1.05	2.63
TPSS-D3(BJ)	7.3	0.40	0.14	1.28/−0.90	2.18
M11-L	18.1	1.10	−0.95	1.09/−4.71	5.80
M11-L-D3(0)	38.4	1.40	−1.40	0.00/−4.45	4.45
BLYP-NL	12.6	0.42	−0.14	1.07/−1.89	2.96
VV10 (rPW86PBE-NL)[b]	10.9	0.41	−0.04	1.38/−1.50	2.88
Amber FF	30.4	1.61	0.85	4.64/−2.72	7.36

[a]The Amber bsc0χ_{OL3} FF results are included for comparison. The reference method is DLPNO−CCSD(T)/CBS*, as defined in the text. The def2-QZVP basis set is used throughout. Alternative analysis using the A-RNA **1a** family as the reference point can be found in the Supporting Information. [b]The VV10 functional is based on the rPW86PBE xc-kernel.

The conventional, additive-estimated CBS extrapolation scheme denoted as ΔCBS uses a high-level correction term, based on focal point analysis[77,78] δ^{HL}_{MP2}

$$\delta^{HL}_{MP2} = E_{HL} - E_{MP2} \quad (4)$$

which is added to the MP2/CBS results.

$$E_{\Delta CBS} = E_{MP2/CBS} + \delta^{HL}_{MP2} \quad (5)$$

Usually, E_{HL} within δ^{HL}_{MP2} is obtained from CCSD(T) calculations, but any level of theory exceeding MP2 can be applied, in principle. For our MP2.5/ΔCBS results, we employ MP3/def2-SVPD as the higher-level correction.

Selection of the Reference Structure for Relative Energies. The selection of the reference point is not straightforward. In QM benchmark studies, it is common to take the most stable conformation as the reference point. In our particular case, this is conformation **2**[, which is close to the B-form conformation in DNA with a shifted β angle value.[5b] This conformation can often be found, e.g., in the RNA kink-turn motif.[79] (The "[" symbol indicates an intercalated shape.) On the other hand, for bioinformatics or force field parametrization purposes, it would be more appropriate to use the biologically dominant conformation **1a**, i.e., the canonical A-RNA. We decided to follow the common benchmark practice and use the lowest energy conformer **2**[as the reference point. The alternative analysis using **1a** as the reference point can be found in the Supporting Information.

The conformational energies show only a static picture of the RNA backbone family energy distribution and should not be mistaken for a biologically relevant stability ordering. The biological stability is dependent greatly on (i) the solvent environment and the overall structural context and (ii) the ensemble representation of the respective backbone family.[8] The idealized structures calculated herein are unlikely the "semiglobal" minima energy structures within the family ensemble representations. From our experience, we expect that structures within a given set of backbone angle boundary conditions, i.e., the particular backbone family, can have an energy spread of several kcal/mol. Note also that the shapes of the PES basins of the individual families can be highly variable. Finer scanning of the conformational space of the individual families is a tedious multidimensional problem that is beyond the scope of this work, but will be targeted in the future. Nonetheless, our specific set of structures can serve as a well-defined benchmark for all fast electronic structure methods and force fields, or hybrids thereof, as we have each known RNA backbone family represented by one well-defined single geometry.

RESULTS AND DISCUSSION

The UpU RNA Benchmark Dataset. The UpU dinucleotide dataset consists of the 46 entries of the consensual list of conformational families present in RNA X-ray structures as derived by Richardson[5b] (cf. Table S4 in the Supporting Information). Although our benchmark energies can be further refined in the future work when more powerful hardware is available (see the explanation in the Computational Details section), our geometries should represent an ultimate and balanced set of structures for comparison of different computational methods over the full spectrum of dinucleotide conformations that may occur in folded RNA molecules.

DOI: 10.1021/acs.jctc.5b00515
J. Chem. Theory Comput. 2015, 11, 4972−4991

Table 2 lists the high-level wave function reference conformational energies obtained with the DLPNO−CCSD-(T)/CBS* protocol,[29] along with a few selected key methods. Many other methods will be discussed on a statistical basis further below. Importantly, Table 2 reveals a good agreement between the DHDF PWPB95-D3(BJ)/def2-QZVP and the reference. This gives us additional confidence in the reference values, since PWPB95-D3(BJ) is known to give reliable results for a wide range of systems and noncovalent interactions in particular. Generally speaking, all three DFT-D3 methods show mutually very consistent results and agree well with the DLPNO−CCSD(T)/CBS* reference. The AMBER force field shows considerably larger differences.

Considering other methods, M06-2X agrees well with the DFT-D3 functionals for most geometries; the effect of the D3(0) correction is often negligible and occasionally worsens the results. However, conformations with stacked nucleobases (e.g., **1a**) benefit greatly from the D3(0) correction, which leads to overall favorable statistics (see Table 3, presented later in this work) for M06-2X-D3, compared to the plain M06-2X. The SCS-MP2/CBS(3,4) method is also in good agreement with the reference and DFT-D3. Note that the statistical performance of SCS-MP2 for noncovalent interactions is usually behind the performance of DHDFs.[72] Mutual agreement between all these higher-level methods is an indication that our data can serve as a reference for simpler low-cost computational methods.

Statistical Analysis of Conformational Energies. *(i). Density Functional Theory.* The typically reported statistical value in QM benchmarks is the mean absolute deviation (MAD). Methods reaching MAD values below the 1 kcal/mol threshold are usually labeled to be of "chemical accuracy". This habit has received some criticism,[80] because the MAD is smaller than the 95% confidence interval ($u_{95\%}$) for an ideal distribution of errors. The MAD value itself is still a robust and valuable statistical measure, just the connection with "chemical accuracy" in the language of statistical uncertainties must be made very carefully.

For comparative reasons with previous work, we also will use MAD in our study. In addition, we will additionally use the mean absolute percent deviation (MAPD), which takes into account the actual magnitude of the reference values:

$$\mathrm{MAPD} = \frac{100}{n} \sum_{n} \frac{|E_{\mathrm{reference}} - E_{\mathrm{functional}}|}{|E_{\mathrm{reference}}|} \qquad (6)$$

where the summation index runs over all 46 systems. In the case of the UpU46 benchmark set, the arithmetic mean of all reference values is ∼7.4 kcal/mol and the maximum value is 18.2 kcal/mol (for **4s**; cf. Table 2). In addition, we use the following statistical measures: the maximal and minimal deviations (max/min dev), the deviation range (devR), and, for completeness, we also use the mean deviation (MD). We consider the MAD, MAPD, and devR values to be the most important values for our benchmark. Since the MAD and MAPD are similar, we will focus more on the MAPD. Note that the devR is independent of the choice of the reference structure while the other measures including MAPD may be affected by the choice of the reference structure.

Table 3 summarizes the statistics using the lowest energy structure **2**[as the reference, while Table S8 in the Supporting Information shows the data recalculated using the A-RNA **1a** structure as the reference. We loosely follow the picture of Jacob's ladder[81] for DF classification, starting with the double hybrid density functionals (DHDFs). DHDFs have been repeatedly reported to deliver highly accurate interaction energies in a large number of benchmark sets.[72] They have also been among the best performing functionals for the earlier RNA rSPS benchmark.[31]

Double Hybrid Density Functionals. The B2PLYP-D3(BJ) functional was the first DHDF proposed.[82] In our UpU RNA benchmark, it reaches approximately the same MAPD as one of the more recently developed DHDFs, the PWPB95-D3(BJ)[72] functional (8.7% vs 9.0%). The PWPB95-D3(BJ) devR of 1.79 kcal/mol is the second lowest of all DFs and is close to the lowest devR of 1.63 kcal/mol obtained by B2GPPLYP-D3(BJ). The "general-purpose" variant of B2PLYP, the B2GPPLYP-D3(BJ)[83] functional, gives also the second lowest MAPD of all DFs with 8.0%. However, the lowest MAD of 0.33 kcal/mol is obtained by DSD-BLYP-D3(BJ). The MAPD is more sensitive to deviations from small reference values than the MAD, which can explain the disparity of having the lowest MAPD and MAD for different functionals. Another important aspect is the aforementioned limited accuracy of our DLPNO−CCSD(T)/CBS* reference, which does not justify a discussion of subtle differences among the DHDFs, as we are likely close to the expected ∼5% error margin of the reference method. The DSD-BYLP-D3(BJ)[84] functional was one of the best performing functionals in the RNA rSPS benchmark and also shows excellent performance herein with an MAPD of 8.6%. DSD-BLYP-D3(BJ) and B2GP-PLYP-D3(BJ) can be identified as the two best performing DHDFs from the tested set of functionals. All DHDFs can be considered to achieve excellent accuracy for the UpU46 benchmark. Taking into account the size of the system and the diversity of the structures, the devR of 2 kcal/mol or less means an excellent mutual agreement of all these methods, and they can be considered to be of similar accuracy.

(Meta-)hybrid and Range-Separated Density Functionals. Compared to DHDFs, we observed a moderate increase in the devR, as well as an increase in the MAPD/MAD values, indicating a small overall decline in the statistical performance for (meta-)hybrid functionals. Statistically, the two best performing (meta-)hybrid functionals are PW6B95-D3(BJ), with an MAPD of 10.5% (MAD = 0.51 kcal/mol), and PBE0-D3(BJ), with an MAPD of 8.4% (MAD = 0.43 kcal/mol). The MAPD performance of PBE0-D3(BJ) reaches almost the DHDF level of accuracy, which seems to be a positive outlier, if compared to the other hybrid functionals. PW6B95-D3(BJ)[24j,85] showed excellent results for many benchmarks in the past,[24j] and the good results for the UpU46 benchmark indicate once again its general robustness. The lowest MAD of the hybrid DFs is given by B3LYP-NL (0.37 kcal/mol), although the devR and MAPD values are comparable with the other hybrid functionals. B3LYP-D3(BJ) usually shows a very good performance for interaction energy benchmarks as the typically over-repulsive LYP-part combines very well with the BJ-damping version of D3.[24k] For the UpU46 set, B3LYP-D3(BJ) shows good overall performance as well, but the MAPD of 12.0% and the devR of 2.5 kcal/mol puts B3LYP-D3(BJ) slightly behind the PW6B95-D3(BJ) functional.

The four included range-separated functionals (RSFs)—M11, ωB97x-D3(0), CAM-B3LYP-D3(BJ), and LC-BOP-LRD—belong to the lower performance spectrum of the hybrid functionals. ωB97x-D3(0) and CAM-B3LYP-D3(BJ) perform similarly, but CAM-B3LYP-D3(BJ) has slightly better overall statistics. While the MAPD of M11 is on par with other

DOI: 10.1021/acs.jctc.5b00515
J. Chem. Theory Comput. 2015, 11, 4972−4991

hybrid functionals (~15%) the MAD of 0.92 and the devR of 3.50 are notably deviating from the usual hybrid functional values. The newly parametrized D3(0) correction for M11 improves the MAD to 0.83 kcal/mol, which is still not competitive with the other tested hybrids. The fourth RSF LC-BOP-LRD yields, besides SOGGA11X, one of the worst statistics with an MAPD of 17.2% (MAD 0.82 kcal/mol) and also the second largest devR of ~4 kcal/mol.

The other two Minnesota functionals, M06-2X and SOGGA11X, show improvement from the D3(0) correction as well. We note that M06-2X already gives good results without the D3 correction, surpassing the aforementioned RSFs in most aspects, but its devR reaches ~3 kcal/mol. Note also that, when using the **1a** structure as the reference (Table S8 in the Supporting Information), the MAD for M06-2X increases from 0.60 kcal/mol to 1.27 kcal/mol. This is one of the few methods showing a noticeable difference between statistical data calculated with different reference points. This is a sign of a specific imbalance in the method and related to the asymptomatically incorrect decay of the incorporated midrange dispersion treatment.[24j,k] As noted above, this becomes visible in stacked conformers such as **1a**. Choosing **1a** as a reference point then leads to a bias that results in the observed MAD differences. Robust methods such as the DHDFs do not show these problems.

Adding the D3(0) correction improves the MAD from a decent value of 0.6 kcal/mol to an excellent value of 0.47 kcal/mol and also reduces the difference between the statistical data calculated using the different reference points. However, the MAD decrease goes hand in hand with an increase in the devR, indicating that the D3(0) correction for M06-2X is not a perfect solution working across all the structures. If we compare the individual energies listed in Table 2, we observe that some conformers are slightly overstabilized, while others are destabilized by the dispersion correction. We think that with the reduction of the MAD, one can justify recommending the dispersion-corrected M06-2X-D3(0) variant over the conventional version for studies of large nucleic acids systems. The typical RNA system has more pronounced base stacking, since the **1a** conformer is the dominant backbone family, and the D3(0) correction becomes more important. Note that uracil is a small nucleobase and studies including purine bases may show increased errors from base stacking as well. Significant improvements from the D3(0) correction are seen for the SOGGA11X functional, whose MAPD gets reduced from 57.9% to 15.6%. Also, the devR improves greatly from ~8 kcal/mol to ~4 kcal/mol. The D3(0) correction is thus deemed necessary for SOGGA11X.

(Meta-)GGA Density Functionals. The treatment of anions may be problematic with semilocal DFs.[86] The exchange-correlation potentials of essentially all semilocal DFs have the same exponential decay as the density instead of $-1/r$, where r is the electron−nucleus distance. This often leads to poorly described HOMO energies and can even lead to formally unbound electrons, resulting in a positive HOMO energy, and is a manifestation of the self-interaction error (SIE)[87] in DFT. The HOMO−LUMO gap for TPSS/def2-QZVP lies between 2 and 3 eV for all UpU conformers, indicating a somewhat problematic description of the electronic structure of the UpU model in the gas-phase. Similar results are obtained for all (meta-)GGA functionals. However, the HOMO energies are negative and thus all electrons are formally bound. The def2-QZVP basis contains semidiffuse functions that do at least partially account for the needs of the net negative charge. Specially designed diffuse functions with even smaller basis set exponents could eventually lead to larger errors with semilocal DFs. Note that hybrid functionals reduce the self-interaction error by partial inclusion of exact Fock exchange and show more physical HOMO−LUMO gaps above 4 eV. Still, we suggest that the anion issue is not a major problem for the application of meta-GGA functionals for nucleic acids, since typical calculations on larger nucleic acid building blocks with more than one negatively charged phosphate would anyway require inclusion of an implicit solvent.[14] The implicit solvation treatment screens the net negative charge and typically increases the HOMO−LUMO gaps. Therefore, our benchmark UpU structures are not significantly affected by unphysically small HOMO−LUMO gaps and the resulting artificial charge transfer, since they are obtained in the presence of a continuum solvent model. We rechecked the older benchmark set with the small rSPS model lacking the nucleobases[31] and found that it is less problematic regarding the HOMO−LUMO gap of the semilocal DFs; typical values of ~4 eV are obtained for TPSS. Introducing the nucleobases seems to increase the self-interaction error in the gas-phase.

The lowest devR value among all (meta-)GGA functionals in Table 3 is reached by the meta-GGA TPSS-D3(BJ) (only 2.18 kcal/mol). It also yields the lowest MAD (0.40 kcal/mol) and the lowest MAPD (7.3%) of all DFs. This puts TPSS-D3(BJ) on the same excellent level of performance as the hybrids M06-2X and PBE0-D3(BJ), but at a much lower computational cost. This high level of accuracy is not expected *a priori* from a meta-GAA functional, because of the self-interaction error discussed above. Considering that the SIE is clearly visible in the HOMO−LUMO gap, it is reasonable to expect that part of the good performance for TPSS-D3 is due to fortuitous error cancellation. The good performance of TPSS-D3(BJ) also may be affected by the fact that this functional has been used to relax the reference structures, albeit in the continuum solvent approximation, diminishing the anion-induced SIE. The good performance of TPSS-D3(BJ) is important since it has been used in our preceding large-scale QM studies on nucleic acid building blocks.[14] Note that TPSS-D3 is the default DFT level for structure optimizations and many routine calculations in the Grimme group for some years.

Most of the other GGAs functionals also show a good performance, being almost on par with the (meta-)hybrid functionals. BLYP-D3(BJ) performs even slightly better than its hybrid B3LYP-D3(BJ) counterpart with an MAPD of 11.2% (MAD = 0.46 kcal/mol). BLYP-NL performs slightly worse than B3LYP-NL: its MAPD is 12.6% (MAD = 0.42 kcal/mol). The VV10 functional—or rPW86PBE-NL in the "−NL" notation—gives statistically better results than BLYP-NL with an MAPD of 10.9% (MAD = 0.41 kcal/mol). The M11-L range-separated meta-GGA does not reach a MAD value of <1 kcal/mol and is on the lower end of the performance spectrum, with an MAPD value of 18.1%. The D3(0) correction does not remedy this fact and actually worsens the results even more, to an MAPD value of 38.4% (MAD = 1.54 kcal/mol), despite the fact that D3 improves the MAD value of the S66 benchmark, as mentioned above.

We also calculated three-body dispersion effects[61,88] for various functionals (not shown), but only found small changes that are too close to the accuracy limits of the reference methods. More accurate reference data are needed before the

DOI: 10.1021/acs.jctc.5b00515
J. Chem. Theory Comput. 2015, 11, 4972−4991

Table 4. Statistical Results for the LQM Methods on the UpU46 Benchmark, Using the 2[Structure as the Reference Point[a]

	MAPD (%)	MAD (kcal/mol)	MD (kcal/mol)	max/min dev (kcal/mol)	devR (kcal/mol)
HF-3c	51.8	2.88	2.78	6.12/−1.86	7.98
PM6	95.0	4.06	3.99	9.02/−1.45	10.47
PM7	45.2	2.37	2.10	9.72/−1.85	11.57
PM6-D3H+	53.5	2.98	2.93	6.70/−0.59	7.28
DFTB3	56.8	2.23	−0.01	6.75/−4.90	11.65
DFTB3-D3(BJ)	28.4	1.26	−0.71	2.22/−3.72	5.95
TPSS-gCP-D3/def2-SVP	26.5	1.17	1.09	3.51/−0.55	4.06
PW6B95-gCP-D3/def2-SVP	25.8	1.36	1.32	3.88/−0.43	4.30
QM^{nb}/MM^{sp} ME	26.5	1.43	0.45	4.43/−2.96	7.39
QM^{nb}/MM^{sp} EE	34.4	2.01	1.68	6.81/−1.68	8.49
QM^{sp}/MM^{nb} ME	24.1	1.05	−0.46	2.07/−3.72	5.79
QM^{sp}/MM^{nb} EE	92.7	4.17	−4.02	2.86/0.00	14.76
Amber FF	30.4	1.61	0.85	4.64/−2.72	7.36

[a]The Amber bsc0χ_{OL3} FF results are included for comparison.

three-body effects can be properly judged. The interested reader can find the current data in the Supporting Information.

Amber RNA Force Field. Table 3 also shows that most modern dispersion-corrected functionals provide more-accurate results than the standard RNA bsc0χ_{OL3} FF. The FF MAPD value of 30.4%, together with the MAD value of 1.61 kcal/mol, are significantly higher than for most DFT/DFT-D3 functionals, with the exception of SOGGA11X and M11-L-D3(0). However, the force field has a considerably larger devR than even the least satisfactory DFT methods. Table 2 reveals that outliers are more pronounced in the FF than in DFT-D3, which is a typical behavior of empirically fitted potentials. This behavior, to some extent, is also visible for the semiempirical methods (see below). These outliers cause an increase in the devR value. Nevertheless, the FF performance is rather impressive for a solely empirical potential that allows routine microsecond-scale MD simulations of complete nucleic acids. Note that the FF employs a set of suboptimal point charges that were not meant to be used in pure gas-phase calculations. Nevertheless, this FF accuracy is insufficient for a quantitatively correct description of RNA molecules and may occasionally fail. Although the FF is known to have a reasonable performance in explicit solvent simulations, we should expect some errors caused by the description of the backbone conformational space, as discussed in the literature.[10b,d,14,89] The large devR value could potentially lead to a qualitatively incorrect description of RNA molecules, if the simulated molecule has a chance to flip to some overstabilized non-native backbone conformation.[10b] The maximum deviation is found for family **6j** and the minimum deviation is found for **2o**. Fortunately, both of these families have a low population in the database used to define the consensus list of backbone families and do not appear to be important for any specific RNA topologies.[5b] Nevertheless, it is not possible to predict the effect of the inaccuracies on the simulations from gas-phase benchmarks *a priori*. In the literature, there are well-documented cases where errors in the description of the dihedral potential energy of <0.5 kcal/mol per suite can entirely degrade the simulated structure of nucleic acids. This happens when the imbalance leads to the unfortunate stabilization of some pathological substates and the pathology is magnified over multiple nucleotides (for example, in regular helical structures).[10b,43b,c] One of the problems that we noticed in our earlier RNA simulations of the Sarcin-Ricin loop RNA motif is that the MM simulations can stabilize spurious backbone conformations that do not correspond to any of the experimentally known 46 RNA backbone families.[14b] It underlines the fact that simple, heavily parametrized methods can show increased errors in certain parts of the PES, because of the accidental loss of error compensation. This is much less likely to happen with high-level methods. RNA backbone conformations predicted by MD simulations, but not seen experimentally, are not included in the present study; we plan to investigate these conformations in the future.

We have also investigated the possibility that the error of the FF energy calculations may be increased by using QM-optimized geometries for the FF energy computations. Thus, we reoptimized the UpU dinucleotides with the bsc0χ_{ol3} FF using a GB implicit solvation model.[90] However, when using these MM-optimized geometries for MM energy computations, i.e., comparing "MM on MM" data with "QM on QM" data, the error, with respect to our reference DLPNO−CCSD(T)/CBS* data, is even slightly further increased to an MAD value of 1.69 kcal/mol and an error range of 7.85 kcal/mol. Thus, the large errors of the FF description of the UpU dinucleotides are indisputable.

Note that there are also other variants of RNA force fields available in the recent literature. One of them is the Yildirim et al. modification (χ_{Yil}) of the χ dihedral angle.[91] Since it is quite similar to the χ_{ol3} correction, we did not repeat the calculations, because the results would be identical to those with χ_{ol3}. Another force field has been described by Chen and Garcia.[92] This version, besides adapting the χ torsion to mimic the overall profile of the earlier χ_{Yil} and χ_{ol3} modifications, tries to tune the simulations by altering van der Waals combination rules of nonbonded interactions between solute and solvent. Since the later modification is applicable only in explicit solvent simulations, it is not relevant to our benchmark gas-phase data. In fact, we assume that all variants of the Cornell et al. force field should perform similarly when tested against the present QM benchmark. The differences between the MM and QM data are very large and do not appear to be resolvable by modest tuning of the dihedral potential functions, which has been a common strategy in recent reparametrizations of the force field. The dihedral potentials are typically parametrized at the very end, in an attempt to implicitly include missing electronic structure effects and somehow compensate for errors in the other force field terms.[10a,b,25] Thus, trying to achieve full agreement between the MM and QM benchmark data by refitting solely the dihedral potentials would likely lead to unrealistic dihedral profiles, which would cause undesired side

DOI: 10.1021/acs.jctc.5b00515
J. Chem. Theory Comput. 2015, 11, 4972−4991

effects. We suggest that, to obtain agreement with the target QM data, a large-scale overhaul of the entire force field would be required, and even this might not guarantee a success. It remains to be resolved by future studies if the agreement between QM and MM can be radically improved in the framework of the present pair-additive force field approximation with constant point charges, lack of explicit electronic structure effects, lack of coupling between the dihedral potentials, and other major approximations. We repeated the MM calculations with CHARMM36,[93] which is the latest version of the pair-additive CHARMM force field for RNA. The differences between the QM and MM descriptions for the UpU46 database are larger, compared to the AMBER force field (see the Supporting Information).

We would like to note that the above paragraphs should in no case be taken as a criticism of the FF methods. Because of the importance of sampling in studies of biopolymers, we desperately need fast computational methods. The closer the fast methods are to the physically correct descriptions, the better our chances are to improve the results in the framework of multiscale modeling combining approaches with different intrinsic accuracy.[14a]

(ii). Low-Cost Quantum Chemical Methods. Table 4 summarizes the performance of low-cost QM (LQM) methods for our UpU46 benchmark database. Performance of LQMs is particularly important for routine QM studies of a system with hundreds of atoms. The term "low-cost" roughly refers to the computational demands and is indirectly defined by a relative comparison to other methods. A common feature among all these methods is an accepted tradeoff between often understood methodological shortcomings and the desire to reduce the computational complexity. We understand the term semiempirical quantum chemical methods (SQMs), which has been frequently used in the literature,[94] as a subset of LQMs. It is debatable if HF-3c is at the same level of empiricism as, e.g., PM6. PM6 replaces matrix elements of the Hamiltonian with empirical values, while HF-3c employs the full electronic Hamiltonian with the addition of correction potentials that are only partially "semiempirical", e.g., the D3 correction components are obtained *ab initio*.[61] A perspective article on LQM methods was recently published.[95]

The HF-3c and PM6/PM7 methods employ essentially a minimal basis set, which artificially confines the anionic charge spatially too close to the valence electrons, especially in the gas phase. These incorrect physics could potentially have a significant impact on the method's performance on the anionic dinucleotides, compared to neutral molecules. A similar problem can be expected for the gCP-corrected def2-SVP calculations. Implicit solvation calculations would suffer less from confining the anion as the overall charge distribution is altered. Applications within a QM/MM electrostatic embedding environment might also alleviate some of the electrostatic problems.

For our RNA benchmark, plain PM6 yields a MAPD of 95.0% and MAD of 4.06 kcal/mol with an error range of >10 kcal/mol, which is larger than for the force field. Adding the D3H+ correction (D3-dispersion plus an hydrogen bond correction) reduces the MAPD to ∼53.5% and the error range to 7 kcal/mol. However, the overall performance of (gas-phase) PM6-D3H+ remains unsatisfactory and, based on this benchmark, RNA studies with PM6-D3H+ are not recommended without further modifications. Similar words can be said about PM7, which shows, compared to PM6-D3H+, a better MAPD (45.2%), but a much worse devR (11.5 kcal/mol).

HF-3c shows slightly improved performance over PM6-D3H+ with an MAPD of 51.8% (MAD = 2.88 kcal/mol) and a similar devR. In a previous study, we recognized a problematic description of the phosphate unit with HF-3c, namely, bond lengthsthat are too short, compared to TPSS-D3.[13] This might negatively influence the single-point energy calculations based on the TPSS-D3 structures as well.

The DFTB3 performance is clearly improved by the D3(BJ) correction, but still remains far from the accuracy of the high-level DFT results displayed in Table 3. Nevertheless, DFTB3-D3 is among the best performing tested LQM methods, with a MAPD value of 28.4%. This makes DFTB3-D3 a potentially viable and cost-effective approach in RNA motif studies.

The gCP-corrected methods are ∼1−2 orders of magnitude slower, compared to, e.g., DFTB3-D3; however, they achieve a better accuracy. The DFT small basis set (def2-SVP) TPSS calculations corrected by gCP and D3(BJ) (denoted by the suffix "-gCP-D3") reach an accuracy that is similar to DFTB3-D3 with an MAPD of 26.5% (MAD = 1.17 kcal/mol). The devR values of ∼4 kcal/mol belong to the lowest devR values among the tested LQMs, indicating a general robustness. PW6B95-gCP-D3/def2-SVP results are comparable to the TPSS-gCP-D3/def2-SVP data, but give slightly worse results overall. Since PW6B95 is computationally more expensive, because of the inclusion of exact Fock exchange, TPSS-gCP-D3 appears to be a better choice. While the performance is unsatisfactory for reliable energy computations, TPSS-gCP-D3 might be suitable for geometry optimizations, which are often slightly less sensitive to the level of theory.

QM/MM partitioning is usually applied to reduce the computational costs and can be accounted to LQMs, in the broader sense, as well. We tested both mechanical (ME) and electrostatic embedding (EE). The two ONIOM-style QM/MM approaches applied herein define the nucleobases as one region, and the sugar−phosphate backbone as the other region. The QM^{nb}/MM^{sp} approach places the nucleobases in the QM region and the backbone in the MM region, and QM^{sp}/MM^{nb} denotes the opposite situation. This way of partitioning is challenging, because both regions are small and the boundary region is large. The errors can thus be considered an upper bound for real applications of QM/MM approaches, where a less extreme partitioning is used. The glycosidic C−N bond is broken and replaced in the link-atom scheme with a hydrogen atom. Breaking up polar bonds should always be done with care. In the case of QM^{nb}, the polarity of the bond is preserved (C replaced by H), whereas, for MM^{nb}, the dipole moment changes because N replaces H. This leads to a significant error, when combined with the EE scheme, with an MAPD value of 92.7%. Interestingly, QM^{sp}/MM^{nb}(ME) gives statistically better results than QM^{nb}/MM^{sp}(ME), despite the unfavorable change of the C−N bond polarity. This may reflect inclusion of the more problematic backbone segment into the QM region. Base stacking is known to be rather well-described by MM, in contrast to the backbone. The overall results for QM^{sp}/MM^{nb}(ME) show an improvement over the Amber FF results with an MAPD of 24.1%, but remain far from the equivalent full QM TPSS-D3 statistics. QM^{nb}/MM^{sp}(ME) is statistically also slightly better than the Amber FF, with a MAPD value of 26.5%. This means that both partitioning schemes with ME improve the FF results, albeit not dramatically. Electrostatic embedding would constitute a more physical description;

DOI: 10.1021/acs.jctc.5b00515
J. Chem. Theory Comput. 2015, 11, 4972−4991

Table 5. Statistical Results from Wave-Function Based Methods on the 46 RNA Backbone Family Conformers

	MAPD (%)	MAD (kcal/mol)	MD (kcal/mol)	max/min dev (kcal/mol)	devR (kcal/mol)
MP2/CBS(3,4)	15.0	0.43	−0.29	0.65/−2.09	2.74
SCS-MP2/CBS(3,4)	11.7	0.47	0.21	1.25/−0.83	2.08
MP2.5/ΔCBS[a]	5.9	0.33	0.14	1.16/−0.60	1.76
MP2-F12/cc-pVDZ-F12	15.9	0.47	−0.32	0.74/−2.10	2.85
MP2/cc-pVDZ	32.2	1.23	0.46	3.07/−4.02	7.09
SCS-MP2/cc-pVDZ	20.7	1.09	0.83	3.38/−1.71	5.09

[a]ΔCBS is based on an additive MP3/def2-SVPD high-level correction to MP2/CBS(3,4).

however, in our particular case, it worsens the results. The EE method explicitly includes polarization of the QM region by the MM region; however, in practice, EE results, in some cases, may be seriously affected by overpolarization effects. We can conclude that none of the tested partitioning schemes, separating bases and backbone, results in a decisive improvement of the calculations over the full MM treatment. Obviously, common utilizations of QM/MM procedures with less drastic partitioning, where a single QM-treated RNA segment would be embedded within a large MM context, are expected to show smaller errors. Work is in progress to test additional QM/MM-based approaches to study nucleic acid building blocks, and the results will be published elsewhere.

In summary, the LQMs show considerably worse performance, compared to high-level dispersion-corrected DFs and no clear improvement compared to the Amber FF.

(iii). Wave Function Methods. Table 5 gives a statistical summary of the results from wave-function-based methods on the 46 RNA backbone family conformers. Because of the system size, the number of applicable wave function methods is limited and, thus, we only include some common ones. It is known that MP2 suffers from strong overestimation of $\pi-\pi$ and CH-π dispersion interactions.[38] Both contributions are present in the UpU dinucleotides to a varying degree in the majority of the conformers. Thus, the MP2/CBS MAPD of 15.0% (MAD = 0.43 kcal/mol) is somewhat higher, compared to that of the best DFT-based methods. There are <10 conformers with substantial stacking, so that this particular error is not influencing the statistics too strongly. However, care must be taken about those systems with stacked nucleobases, such as the A-form RNA family **1a**, where the particular error for MP2/CBS(3,4) is 1.5 kcal/mol. For the older rSPS RNA benchmark lacking the nucleobases, MP2/CBS gave results close to the CCSD(T) reference.[31] Thus, the MP2/CBS errors for the UpU46 dataset primarily stem from an imbalanced description of base stacking. Similar to the situation with M06-2X noted earlier, the MAD decreases to 1.19 kcal/mol when using the stacked conformer **1a** as a reference point.

MP2 is known to be very dependent on the basis set, but some studies still employ only double-ζ basis sets at the MP2 level, hoping for error cancellation. A recent study discussed this issue in the context of tetrapeptide conformations.[96] The MP2/cc-pVDZ calculations for the UpU46 benchmark system lead to the expected worsening of the statistical performance. The MAPD of 32.2% illustrates why MP2/"small basis set" calculations are definitely not advised for biomolecular structures.

Improvement compared to MP2/CBS is observed by SCS-MP2/CBS with MAPD = 11.7%, showing a performance similar to that of hybrid DFT-D3 functionals, but still behind DHDFs. Again, the small cc-pVDZ bases set deteriorates the accuracy of SCS-MP2 to 20.7%.

Explicitly correlated methods take the interelectronic distance explicitly into account.[39] Several variants of these methods have been proposed in the literature, and we only take a look at MP2-F12 calculations as implemented in ORCA.[97] It could be shown, for various benchmarks, that the F12 approach greatly reduces the BSSE for intermolecular interactions and that triple-ζ results achieve a higher accuracy at a lower computational cost, compared to a MP2/CBS(4,5) extrapolation.[97] It is known that explicitly correlated methods show less dependency on the basis set, and that the results obtained from MP2-F12 are similar to the results obtained from canonical MP2 with a by one higher cardinal number basis set. Thus, MP2-F12/DZ is expected to give at least MP2/TZ quality results.[39] However, a major drawback is an increase in computational complexity. Our results using MP2-F12/cc-pVDZ show a significantly lower MAPD, compared to MP2/DZ with 15.9% (MAD = 0.47 kcal/mol), reaching almost the same values as MP2/CBS.

The MP2.5/ΔCBS results are in very good agreement with the DLPNO−CCSD(T)/CBS* values with MAPD = 5.9%, which is the lowest among all tested methods. Also, the MAD value of 0.33 kcal/mol is one of the lowest and is equal to that of DSD-BLYP-D3(BJ). As such, we can recommend MP2.5/ΔCBS as a viable alternative, wave-function-based method for highly accurate results. However, the computational costs of the canonical MP3/def2-SVPD computations are quite considerable, and already for our UpU dinucleotides, the DLPNO−CCSD(T)/def2-TZVP method requires less computational resources. From the methodological point of view, CCSD(T) is obviously preferable over MP3, because of the inclusion of higher-order correlation effects. Nevertheless, the consistency between the MP2.5/ΔCBS and DLNO−CCSD(T)/CBS* data is another indirect justification of our reference method.

Density Functional Theory with Implicit Solvation. From the biological point of view, one of the major drawbacks of the presented calculations is the gas-phase charge distribution. Biomolecules are surrounded by an aqueous environment that also contains ions. This influences the charge distribution, compared to the gas-phase, and also screens the diffuse anionic charge of the phosphate unit. The standard way to treat the charge-screening effects in quantum chemistry is by using implicit solvation models, such as COSMO. This treatment neglects any explicit solute−solvent interactions such as water binding and direct (inner-shell) binding of ions, although the later interaction occurs primarily only in very specific ion-binding pockets.[98] Inclusion of such explicit interactions into QM calculations can sometimes improve the results and should be considered on a case-by-case basis.[14a]

Although the main purpose of our study was to derive a set of benchmark structures of RNA dinucleotides, which justifies the subsequent single-point gas-phase energy calculations, for the sake of completeness, we also report a set of continuum

DOI: 10.1021/acs.jctc.5b00515
J. Chem. Theory Comput. 2015, 11, 4972−4991

Table 6. Statistical Results from Implicit Solvation (COSMO) on a Selected Set of Methods for All 46 UpU Conformers, Using the 1a Family as the Reference Point[a]

	MAPD (%)	MAD (kcal/mol)	MD (kcal/mol)	max/min dev (kcal/mol)	devR (kcal/mol)
PWPB95-D3(BJ)	22.9	0.72	−0.65	0.51/−1.71	2.22
B2PLYP-D3(BJ)	19.3	0.65	−0.59	0.53/−1.63	2.16
PW6B95-D3(BJ)	31.6	0.94	−0.90	0.48/−1.92	2.40
B3LYP-NL	21.0	0.62	−0.53	0.59/−1.97	2.56
B3LYP-D3(BJ)	26.7	0.85	−0.82	0.43/−1.99	2.43
M06-2X	44.5	1.55	−1.51	0.48/−3.27	3.75
M06-2X-D3(0)	27.5	0.87	−0.79	0.71/−2.29	3.00
TPSS-D3(BJ)	23.7	0.83	−0.80	0.36/−1.90	2.26
MP2/CBS(3,4)	31.9	0.95	0.88	1.97/−1.22	3.19
SCS-MP2/CBS(3,4)	25.9	0.92	−0.87	0.40/−2.52	2.92
HF-3c	86.4	2.31	−2.23	1.34/−5.99	7.33
PM6-D3H+	90.6	2.67	−2.62	0.73/−5.77	6.49
PW6B95-gCP-D3(BJ)/def2-SVP	61.3	1.91	−1.87	0.50/−3.68	4.18
TPSS-gCP-D3(BJ)/def2-SVP	53.0	1.80	−1.72	0.83/−3.70	4.53

[a]The def2-QZVP is employed unless noted otherwise. The reference method is DLPNO−CCSD(T)/CBS*.

solvent energy calculations. Obviously, although the continuum solvent shifts the energy evaluations closer to the biochemically relevant environment, the inclusion of continuum solvent also brings additional sources of uncertainty into the computations, which complicates using such data for benchmark purposes. In addition, robust computational methods should describe the molecules correctly, irrespective of the environment, since the exposure of different parts of the nucleic acids molecules to the solvent is context-dependent and variable. Nevertheless, any future QM studies of nucleic model systems with more than one phosphate will have to be done with the inclusion of a solvent, either implicitly, or using QM/MM approaches. The presence of two or more phosphates would bias all energy trends in the gas-phase by long-range ion−ion electrostatics.

The DLPNO−CCSD(T)/CBS* method is again used as the reference for the implicit solvation calculations. The solvation effects are only treated at the SCF level, i.e., by employing "solvated" HF orbitals. This is the accepted standard procedure to obtain correlated energies with implicit solvation, but it leads to a nonstationary energy with respect to the COSMO potential.[99]

The data are summarized in Table 6, and the individual energies are given in Table S7 in the Supporting Information. Several things are notable. First, upon the inclusion of a solvent, we obtain the biological dominant family **1a** as the lowest energy conformation, which will be used as our new reference point. This is in excellent agreement with experiments, since NMR benchmark experiments on unstructured RNA single-strand tetranucleotides indeed show the **1a** A-RNA conformation as dominant in water.[10c] Variability of the energies is greatly reduced, compared to the gas-phase data. The COSMO environment gives a maximum relative energy value of 9.6 kcal/mol with an arithmetic mean of 4.2 kcal/mol. The gas-phase calculations give a maximum value of 18.2 kcal/mol and an arithmetic mean of 7.4 kcal/mol. For these reasons, the magnitudes of the statistical measures for the continuum solvent calculations are not fully comparable with the gas-phase statistics. The devR is of comparable magnitude to the gas-phase data. The MAPD and MAD values for COSMO are larger, compared to the those of the gas-phase, indicating an overall increase in the (mean) deviations. A peculiar point is a systematic shift of ∼0.5−1.0 kcal/mol for DFT-D3 in the mean deviations, cf. with the respective gas-phase data using the **1a** conformer in Table S8 in the Supporting Information. It may reflect some uncertainty of the COSMO model. Nevertheless, the inclusion of COSMO solvation effects does not change any of the conclusions derived from the gas-phase calculations discussed in the first part of the study. The gas-phase and continuum solvent calculations lead to identical ranking of the methods.

SUMMARY AND CONCLUDING REMARKS

A QM structure-energy benchmark study is presented on 46 UpU dinucleotide conformers comprising the complete consensus list of the RNA backbone family classification.[5b] Note that RNA structure, function, and evolution are critically affected by the conformational substates of the RNA backbone.[5b,10b] The role of nucleic acids backbone has been until now severely underestimated in QM literature, which has been typically focused on studies of base stacking and base pairing. Our studied system is considerably more complete than systems previously used for QM benchmark purposes, which, until now, considered base−base interactions and backbone conformations separately.

The geometries of our UpU46 benchmark are derived through restrained[13] COSMO TPSS-D3/def2-TZVP optimizations and cover the complete set of RNA dinucleotide structures presently known from X-ray studies of folded RNAs such as ribosomes.[5b] Utilization of the restrained optimization protocol is an absolutely essential part of our study. The restraints allow us to relax the geometries for subsequent accurate energy calculations while avoiding any significant deviations from the biochemically relevant geometries and formation of any non-native interactions that would bias the subsequent reference energy calculations. We explain in detail why unrestrained or fully constrained optimizations are entirely unsuitable for derivation of structures for accurate QM calculations of dinucleotides. Biochemical relevance of our final structures, i.e., the complete set of RNA backbone families, is explained in detail in the literature.[5b,10b]

Our study brings three sets of results. First, we derive the representative UpU geometries. Second, we calculate the UpU46 benchmark database (i.e., a set of structure−energy points that can be used for assessment of performance of other computational methods). Finally, we test ∼30 different computational methods using the database.

DOI: 10.1021/acs.jctc.5b00515
J. Chem. Theory Comput. 2015, 11, 4972−4991

As the reference method to calculate the energies, we use the DLPNO−CCSD(T) method with a new multiplicative complete basis set extrapolation, marked as DLNPO−CCSD-(T)/CBS*. All method details are given in the Computational Details section. We decided to not use the conventional estimated CCSD(T)/CBS benchmark method for several reasons that are in detail explained in the Computational Details section. Our reference energy calculations are probably somewhat less accurate, compared to CCSD(T)/CBS calculations that are affordable for small systems. Nevertheless, the almost perfect agreement with several additional high-quality methods that are based on different approximations, such as double-hybrid DFs and MP2.5/ΔCBS, strongly supports the correctness of our approach. The data are of sufficient accuracy to serve as the benchmark for any lower-cost computational method.

Various dispersion-corrected DFT functionals, low-cost QM methods and high-level wave function methods are benchmarked against the UpU46 benchmark and compared to the performance of the RNA Amber FF (bsc0χ_{ol3}). The basic result of our work is that the agreement with the UpU46 database deteriorates with reduction of the cost of the QM method. While high-quality methods can very well reproduce the benchmark data, low-cost methods are struggling.

Most large-basis set dispersion-corrected DFT methods give excellent results for the conformational energies, with MAPDs and MADs below 15% and 1 kcal/mol, respectively. The best agreement with the reference data is achieved by DHDF methods, with deviation ranges of <2 kcal/mol and MADs in the 0.3−0.4 kcal/mol range (MAPD = 8%−9%). The best performing hybrid DFT functionals are PW6B95-D3(BJ) and PBE0-D3(BJ) with MAPD values below or close to 10%. The meta-GGA TPSS-D3(BJ) yields the lowest MAPD among all DFT methods (7.3%), although it might be due to cancellation of the errors. B3LYP-NL is a viable alternative to the D3 approach and surpasses B3LYP-D3.

New D3(0) parameters for M11, SOGGA11X, and M11-L are presented. The M06-2X, M11, and SOGAA11X DFs benefit, to varying degrees, from adding the D3(0) dispersion term. However, these methods generally appear to be less reliable than the best dispersion-corrected DFT approaches.

The Amber FF exhibits an MAPD value of 30.4% and a deviation range of >7 kcal/mol. It is a very good performance, considering the simplicity of the force field, but it is still likely to cause imbalances in MD simulations, as documented in the literature.[10a,b,d,13,14,25]

None of the tested low-cost QM methods achieves accuracy comparable to that of the high-quality dispersion-corrected DFT methods. Unfortunately, these methods offer no visible improvement, compared to the MM treatment. We nevertheless found that DFTB3-D3(BJ) is significantly better (MAPD = 28.4%), compared to HF-3c, PM6-D3H+, and PM7. We also suggest that TPSS-gCP-D3/def2-SVP level could be a viable option for QM geometry optimizations of larger nucleic acid building blocks. Although its accuracy falls notably behind large basis-set DFT calculations, it shows reasonable robustness by having the smallest deviation range among the tested lower-level and small-basis-set QM methods.

Neither MP2/CBS(3,4) nor SCS-MP2/CBS(3,4) reach the accuracy of the best DFT methods. SCS-MP2 is only marginally better than MP2. Usage of MP2 or SCS-MP2 with a double-ζ basis set leads to an imbalanced description and is not recommended. MP2-F12 alleviates the basis set dependency and gives results similar to MP2/CBS, but is comparably expensive, because of a significantly larger scaling prefactor.

MP2.5/ΔCBS shows the closest agreement with the DLNPO−CCSD(T)/CBS* reference among the wave function methods, slightly surpassing even the DHDFs, albeit at computational costs that are, in a canonical implementation, at least equal to the DLPNO−CCSD(T)/CBS* calculations.

In conclusion, many high-quality QM methods are capable to neatly reproduce the relative energies of different RNA dinucleotide conformations over the full range of geometries occurring in real RNA structures. However, such calculations are still relatively costly and allow only limited sampling of the conformational space of larger nucleic acids fragments. Since high-level DFT-D3 calculations are accurate enough to pinpoint particular errors in the force fields, they can be used as a complementary tool alongside molecular dynamics simulations to refine the force field energy description, e.g., by analyzing specific structures or molecular interactions.[14a] Unfortunately, we did not find a low-cost QM method of comparable accuracy that would allow for a much broader investigation of the conformational space of larger nucleic acid building blocks. Development of such QM methods, even specifically parametrized for nucleic acids, would be quite vital for the application of QM calculations to larger fragments of nucleic acids. Our UpU46 benchmark can be readily used for testing and eventually parametrization of fast QM methods and nucleic acid force fields, including the emerging polarization ones.[100] Note that, for testing purposes, restrained reoptimizations of the dinucleotide structures using the tested method can be considered before executing the energy calculations.

■ ASSOCIATED CONTENT

Supporting Information

The Supporting Information is available free of charge on the ACS Publications website at DOI: 10.1021/acs.jctc.5b00515.

D3(0) parameters for the M11-L, M11, and SOGGA11-X functionals; relative energies for all presented methods; clustering-mean values of the backbone family classification; Example control file for xopt; details on the unrestrained optimizations for all families; CHARMM36 data (PDF)

Cartesian coordinates of all 46 structures in PDB and XYZ format; text file with reference energies (ZIP)

■ AUTHOR INFORMATION

Corresponding Authors

*E-mail: kruse@ibp.cz (H. Kruse).
*E-mail: grimme@thch.uni-bonn.de (S. Grimme).
*E-mail: sponer@ncbr.muni.cz (J. Sponer).

Notes

The authors declare no competing financial interest.

■ ACKNOWLEDGMENTS

This work was supported by the Grant Agency of the Czech Republic (Grant No. P305/12/G034), by the European Regional Development Fund project "CEITEC—Central European Institute of Technology" (No. CZ.1.05/1.1.00/02.0068) and by the EU Seventh Framework Programme under the "Capacities" specific program (Contract No. 286154). The Praemium Academiae Award, which was provided by the Czech Academy of Science and awarded to J.S., is gratefully acknowledged.

DOI: 10.1021/acs.jctc.5b00515
J. Chem. Theory Comput. 2015, 11, 4972−4991

REFERENCES

(1) (a) Birney, E., et al. (Encode Project Consortium). *Nature* **2007**, *447* (7146), 799−816. (b) Carninci, P. Tagging mammalian transcription complexity. *Trends Genet.* **2006**, *22* (9), 501−510. (c) Pheasant, M.; Mattick, J. S. Raising the estimate of functional human sequences. *Genome Res.* **2007**, *17* (9), 1245−1253. (d) *Non-Protein Coding RNAs*; Springer: Berlin, Heidelberg, Germany, 2009. (e) Bu, D.; Yu, K.; Sun, S.; Xie, C.; Skogerbo, G.; Miao, R.; Xiao, H.; Liao, Q.; Luo, H.; Zhao, G.; Zhao, H.; Liu, Z.; Liu, C.; Chen, R.; Zhao, Y. NONCODE v3.0: integrative annotation of long noncoding RNAs. *Nucleic Acids Res.* **2012**, *40*, D210−D215. (f) Quek, X. C.; Thomson, D. W.; Maag, J. L.; Bartonicek, N.; Signal, B.; Clark, M. B.; Gloss, B. S.; Dinger, M. E. lncRNAdb v2.0: expanding the reference database for functional long noncoding RNAs. *Nucleic Acids Res.* **2015**, *43*, D168−D173. (g) Morris, K. V.; Mattick, J. S. The rise of regulatory RNA. *Nat. Rev. Genet.* **2014**, *15* (6), 423−437.

(2) Mathews, D. H.; Turner, D. H. Prediction of RNA secondary structure by free energy minimization. *Curr. Opin. Struct. Biol.* **2006**, *16* (3), 270−278.

(3) (a) Nissen, P.; Ippolito, J. A.; Ban, N.; Moore, P. B.; Steitz, T. A. RNA tertiary interactions in the large ribosomal subunit: the A-minor motif. *Proc. Natl. Acad. Sci. U. S. A.* **2001**, *98* (9), 4899−4903. (b) Stombaugh, J.; Zirbel, C. L.; Westhof, E.; Leontis, N. B. Frequency and isostericity of RNA base pairs. *Nucleic Acids Res.* **2009**, *37* (7), 2294−2312. (c) Leontis, N. B.; Stombaugh, J.; Westhof, E. The non-Watson−Crick base pairs and their associated isostericity matrices. *Nucleic Acids Res.* **2002**, *30* (16), 3497−3531.

(4) (a) Petrov, A. I.; Zirbel, C. L.; Leontis, N. B. Automated classification of RNA 3D motifs and the RNA 3D Motif Atlas. *RNA* **2013**, *19* (10), 1327−1340. (b) Sponer, J.; Sponer, J. E.; Petrov, A. I.; Leontis, N. B. Quantum Chemical Studies of Nucleic Acids Can We Construct a Bridge to the RNA Structural Biology and Bioinformatics Communities? *J. Phys. Chem. B* **2010**, *114* (48), 15723−15741.

(5) (a) Lu, X. J.; Olson, W. K.; Bussemaker, H. J. The RNA backbone plays a crucial role in mediating the intrinsic stability of the GpU dinucleotide platform and the GpUpA/GpA miniduplex. *Nucleic Acids Res.* **2010**, *38* (14), 4868−4876. (b) Richardson, J. S.; Schneider, B.; Murray, L. W.; Kapral, G. J.; Immormino, R. M.; Headd, J. J.; Richardson, D. C.; Ham, D.; Hershkovits, E.; Williams, L. D.; Keating, K. S.; Pyle, A. M.; Micallef, D.; Westbrook, J.; Berman, H. M. RNA backbone: Consensus all-angle conformers and modular string nomenclature (an RNA Ontology Consortium contribution). *RNA* **2008**, *14* (3), 465−481.

(6) Bida, J. P.; Das, R. Squaring theory with practice in RNA design. *Curr. Opin. Struct. Biol.* **2012**, *22* (4), 457−466.

(7) Chawla, M.; Abdel-Azeim, S.; Oliva, R.; Cavallo, L. Higher order structural effects stabilizing the reverse Watson−Crick Guanine-Cytosine base pair in functional RNAs. *Nucleic Acids Res.* **2014**, *42* (2), 714−726.

(8) Mladek, A.; Sponer, J. E.; Kulhanek, P.; Lu, X. J.; Olson, W. K.; Sponer, J. Understanding the Sequence Preference of Recurrent RNA Building Blocks Using Quantum Chemistry: The Intrastrand RNA Dinucleotide Platform. *J. Chem. Theory Comput.* **2012**, *8* (1), 335−347.

(9) Cragnolini, T.; Laurin, Y.; Derreumaux, P.; Pasquali, S. Coarse-Grained HiRE-RNA Model for ab Initio RNA Folding beyond Simple Molecules, Including Noncanonical and Multiple Base Pairings. *J. Chem. Theory Comput.* **2015**, *11* (7), 3510−3522.

(10) (a) Sponer, J.; Banas, P.; Jurecka, P.; Zgarbova, M.; Kuhrova, P.; Havrila, M.; Krepl, M.; Stadlbauer, P.; Otyepka, M. Molecular Dynamics Simulations of Nucleic Acids. From Tetranucleotides to the Ribosome. *J. Phys. Chem. Lett.* **2014**, *5* (10), 1771−1782. (b) Sponer, J.; Mladek, A.; Sponer, J. E.; Svozil, D.; Zgarbova, M.; Banas, P.; Jurecka, P.; Otyepka, M. The DNA and RNA sugar-phosphate backbone emerges as the key player. An overview of quantum-chemical, structural biology and simulation studies. *Phys. Chem. Chem. Phys.* **2012**, *14* (44), 15257−15277. (c) Yildirim, I.; Stern, H. A.; Tubbs, J. D.; Kennedy, S. D.; Turner, D. H. Benchmarking AMBER Force Fields for RNA: Comparisons to NMR Spectra for Single-Stranded r(GACC) Are Improved by Revised χ Torsions. *J. Phys. Chem. B* **2011**, *115* (29), 9261−9270. (d) Henriksen, N. M.; Roe, D. R.; Cheatham, T. E. Reliable Oligonucleotide Conformational Ensemble Generation in Explicit Solvent for Force Field Assessment Using Reservoir Replica Exchange Molecular Dynamics Simulations. *J. Phys. Chem. B* **2013**, *117* (15), 4014−4027.

(11) Sweeney, B. A.; Roy, P.; Leontis, N. B. An introduction to recurrent nucleotide interactions in RNA. *Wires Rna* **2015**, *6* (1), 17−45.

(12) Hobza, P. Calculations on Noncovalent Interactions and Databases of Benchmark Interaction Energies. *Acc. Chem. Res.* **2012**, *45* (4), 663−672.

(13) Kruse, H.; Sponer, J. Towards biochemically relevant QM computations on nucleic acids: controlled electronic structure geometry optimization of nucleic acid structural motifs using penalty restraint functions. *Phys. Chem. Chem. Phys.* **2015**, *17* (2), 1399−1410.

(14) (a) Šponer, J.; Mládek, A.; Špačková, N.; Cang, X.; Cheatham, T. E.; Grimme, S. Relative Stability of Different DNA Guanine Quadruplex Stem Topologies Derived Using Large-Scale Quantum-Chemical Computations. *J. Am. Chem. Soc.* **2013**, *135* (26), 9785−9796. (b) Kruse, H.; Havrila, M.; Šponer, J. QM Computations on Complete Nucleic Acids Building Blocks: Analysis of the Sarcin−Ricin RNA Motif Using DFT-D3, HF-3c, PM6-D3H, and MM Approaches. *J. Chem. Theory Comput.* **2014**, *10* (6), 2615−2629.

(15) Svozil, D.; Sponer, J. E.; Marchan, I.; Perez, A.; Cheatham, T. E.; Forti, F.; Luque, F. J.; Orozco, M.; Sponer, J. Geometrical and electronic structure variability of the sugar-phosphate backbone in nucleic acids. *J. Phys. Chem. B* **2008**, *112* (27), 8188−8197.

(16) (a) Saenger, W. *Principles of Nucleic Acid Structure*; Springer: New York, 1984 (ISBN: 978-0-38-790761-1). (b) Neidle, S. *Principles of Nucleic Acid Structure*; Elsevier: Amsterdam, 2008 (ISBN 978-0-12-369507-9). (c) Xia, T. B.; SantaLucia, J., Jr.; Burkard, M. E.; Kierzek, R.; Schroeder, S. J.; Jiao, X. Q.; Cox, C.; Turner, D. H. Thermodynamic parameters for an expanded nearest-neighbor model for formation of RNA duplexes with Watson−Crick base pairs. *Biochemistry* **1998**, *37* (42), 14719−14735. (d) Zhurkin, V. B.; Poltev, V. I.; Florent'ev, V. L. Atom−atomic potential functions for conformational calculations of nucleic acids. *Mol. Biol. (Moscow)* **1980**, *14* (5), 1116−1130. (e) Yakovchuk, P.; Protozanova, E.; Frank-Kamenetskii, M. D. Base-stacking and base-pairing contributions into thermal stability of the DNA double helix. *Nucleic Acids Res.* **2006**, *34* (2), 564−574.

(17) (a) Grimme, S.; Djukic, J. P. Cation−Cation "Attraction": When London Dispersion Attraction Wins over Coulomb Repulsion. *Inorg. Chem.* **2011**, *50* (6), 2619−2628. (b) Ehrlich, S.; Moellmann, J.; Grimme, S. Dispersion-Corrected Density Functional Theory for Aromatic Interactions in Complex Systems. *Acc. Chem. Res.* **2013**, *46* (4), 916−926.

(18) Sponer, J.; Sponer, J. E.; Mladek, A.; Jurecka, P.; Banas, P.; Otyepka, M. Nature and Magnitude of Aromatic Base Stacking in DNA and RNA: Quantum Chemistry, Molecular Mechanics, and Experiment. *Biopolymers* **2013**, *99* (12), 978−988.

(19) (a) Condon, D. E.; Kennedy, S. D.; Mort, B. C.; Kierzek, R.; Yildirim, I.; Turner, D. H. Stacking in RNA: NMR of Four Tetramers Benchmark Molecular Dynamics. *J. Chem. Theory Comput.* **2015**, *11* (6), 2729−2742. (b) Roe, D. R.; Bergonzo, C.; Cheatham, T. E. Evaluation of Enhanced Sampling Provided by Accelerated Molecular Dynamics with Hamiltonian Replica Exchange Methods. *J. Phys. Chem. B* **2014**, *118* (13), 3543−3552. (c) Jafilan, S.; Klein, L.; Hyun, C.; Florian, J. Intramolecular Base Stacking of Dinucleoside Monophosphate Anions in Aqueous Solution. *J. Phys. Chem. B* **2012**, *116* (11), 3613−3618. (d) Brown, R. F.; Andrews, C. T.; Elcock, A. H. Stacking Free Energies of All DNA and RNA Nucleoside Pairs and Dinucleoside-Monophosphates Computed Using Recently Revised AMBER Parameters and Compared with Experiment. *J. Chem. Theory Comput.* **2015**, *11* (5), 2315−2328.

(20) (a) Krepl, M.; Otyepka, M.; Banas, P.; Sponer, J. Effect of Guanine to Inosine Substitution on Stability of Canonical DNA and RNA Duplexes: Molecular Dynamics Thermodynamics Integration

DOI: 10.1021/acs.jctc.5b00515
J. Chem. Theory Comput. 2015, 11, 4972−4991

Study. *J. Phys. Chem. B* **2013**, *117* (6), 1872−1879. (b) Koller, A. N.; Bozilovic, J.; Engels, J. W.; Gohlke, H. Aromatic N versus aromatic F: bioisosterism discovered in RNA base pairing interactions leads to a novel class of universal base analogs. *Nucleic Acids Res.* **2010**, *38* (9), 3133−3146. (c) Beierlein, F. R.; Kneale, G. G.; Clark, T. Predicting the Effects of Basepair Mutations in DNA−Protein Complexes by Thermodynamic Integration. *Biophys. J.* **2011**, *101* (5), 1130−1138. (d) Satpati, P.; Åqvist, J. Why base tautomerization does not cause errors in mRNA decoding on the ribosome. *Nucleic Acids Res.* **2014**, *42* (20), 12876−12884. (e) Norberg, J.; Nilsson, L. Conformational free energy landscape of ApApA from molecular dynamics simulations. *J. Phys. Chem.* **1996**, *100* (7), 2550−2554.

(21) Abrams, C.; Bussi, G. Enhanced Sampling in Molecular Dynamics Using Metadynamics, Replica-Exchange, and Temperature-Acceleration. *Entropy* **2014**, *16* (1), 163−199.

(22) Grimme, S. Density functional theory with London dispersion corrections. *Wiley Interdiscip. Rev.: Comput. Mol. Sci.* **2011**, *1* (2), 211−228.

(23) (a) Churchill, C. D. M.; Wetmore, S. D. Developing a computational model that accurately reproduces the structural features of a dinucleoside monophosphate unit within B-DNA. *Phys. Chem. Chem. Phys.* **2011**, *13* (36), 16373−16383. (b) Millen, A. L.; Kamenz, B. L.; Leavens, F. M. V.; Manderville, R. A.; Wetmore, S. D. Conformational Flexibility of C8-Phenoxylguanine Adducts in Deoxydinucleoside Monophosphates. *J. Phys. Chem. B* **2011**, *115* (44), 12993−13002. (c) Hart, K.; Foloppe, N.; Baker, C. M.; Denning, E. J.; Nilsson, L.; Mackerell, A. D., Jr. Optimization of the CHARMM additive force field for DNA: Improved treatment of the BI/BII conformational equilibrium. *J. Chem. Theory Comput.* **2012**, *8* (1), 348−362. (d) Foloppe, N.; MacKerell, A. D. Contribution of the phosphodiester backbone and glycosyl linkage intrinsic torsional energetics to DNA structure and dynamics. *J. Phys. Chem. B* **1999**, *103* (49), 10955−10964. (e) Poltev, V.; Anisimov, V. M.; Danilov, V. I.; Garcia, D.; Sanchez, C.; Deriabina, A.; Gonzalez, E.; Rivas, F.; Polteva, N. The Role of Molecular Structure of Sugar-Phosphate Backbone and Nucleic Acid Bases in the Formation of Single-Stranded and Double-Stranded DNA Structures. *Biopolymers* **2014**, *101* (6), 640−650. (f) Barone, G.; Fonseca Guerra, C.; Bickelhaupt, F. M. B-DNA Structure and Stability as Function of Nucleic Acid Composition: Dispersion-Corrected DFT Study of Dinucleoside Monophosphate Single and Double Strands. *ChemistryOpen* **2013**, *2* (5−6), 186−193. (g) Kubar, T.; Jurecka, P.; Cerny, J.; Rezac, J.; Otyepka, M.; Valdes, H.; Hobza, P. Density-functional, density-functional tight-binding, and wave function calculations on biomolecular systems. *J. Phys. Chem. A* **2007**, *111* (26), 5642−5647. (h) Witts, R. N.; Hopson, E. C.; Koballa, D. E.; Van Boening, T. A.; Hopkins, N. H.; Patterson, E. V.; Nagan, M. C. Backbone-Base Interactions Critical to Quantum Stabilization of Transfer RNA Anticodon Structure. *J. Phys. Chem. B* **2013**, *117* (25), 7489−7497. (i) Foloppe, N.; Hartmann, B.; Nilsson, L.; MacKerell, A. D., Jr. Intrinsic Conformational Energetics Associated with the Glycosyl Torsion in DNA: A Quantum Mechanical Study. *Biophys. J.* **2002**, *82* (3), 1554−1569.

(24) (a) Cooper, V. R.; Thonhauser, T.; Puzder, A.; Schroder, E.; Lundqvist, B. I.; Langreth, D. C. Stacking interactions and the twist of DNA. *J. Am. Chem. Soc.* **2008**, *130* (4), 1304−1308. (b) Mukherjee, S.; Kailasam, S.; Bansal, M.; Bhattacharyya, D. Stacking Interactions in RNA and DNA: Roll-Slide Energy Hyperspace for Ten Unique Dinucleotide Steps. *Biopolymers* **2015**, *103* (3), 134−147. (c) Parker, T. M.; Hohenstein, E. G.; Parrish, R. M.; Hud, N. V.; Sherrill, C. D. Quantum-Mechanical Analysis of the Energetic Contributions to π Stacking in Nucleic Acids versus Rise, Twist, and Slide. *J. Am. Chem. Soc.* **2013**, *135* (4), 1306−1316. (d) Oliva, R.; Cavallo, L.; Tramontano, A. Accurate energies of hydrogen bonded nucleic acid base pairs and triplets in tRNA tertiary interactions. *Nucleic Acids Res.* **2006**, *34* (3), 865−879. (e) Poater, J.; Swart, M.; Bickelhaupt, F. M.; Fonseca Guerra, C. B-DNA structure and stability: the role of hydrogen bonding, $\pi-\pi$ stacking interactions, twist-angle, and solvation. *Org. Biomol. Chem.* **2014**, *12* (26), 4691−4700. (f) Luo, R.; Gilson, H. S. R.; Potter, M. J.; Gilson, M. K. The physical basis of nucleic acid base stacking in water. *Biophys. J.* **2001**, *80* (1), 140−148. (g) Langner, K. M.; Sokalski, W. A.; Leszczynski, J. Intriguing relations of interaction energy components in stacked nucleic acids. *J. Chem. Phys.* **2007**, *127* (11), 11110210.1063/1.2786983 (h) Swart, M.; van der Wijst, T.; Fonseca Guerra, C.; Bickelhaupt, F. M. $\pi-\pi$ stacking tackled with density functional theory. *J. Mol. Model.* **2007**, *13* (12), 1245−1257. (i) Rezac, J.; Riley, K. E.; Hobza, P. S66: A Well-balanced Database of Benchmark Interaction Energies Relevant to Biomolecular Structures. *J. Chem. Theory Comput.* **2011**, *7* (8), 2427−2438. (j) Goerigk, L.; Grimme, S. A thorough benchmark of density functional methods for general main group thermochemistry, kinetics, and noncovalent interactions. *Phys. Chem. Chem. Phys.* **2011**, *13* (14), 6670−6688. (k) Goerigk, L.; Kruse, H.; Grimme, S. Benchmarking Density Functional Methods against the S66 and S66 × 8 Datasets for Non-Covalent Interactions. *ChemPhysChem* **2011**, *12* (17), 3421−3433.

(25) Sponer, J.; Cang, X. H.; Cheatham, T. E. Molecular dynamics simulations of G-DNA and perspectives on the simulation of nucleic acid structures. *Methods* **2012**, *57* (1), 25−39.

(26) Goerigk, L.; Grimme, S. A General Database for Main Group Thermochemistry, Kinetics, and Noncovalent Interactions—Assessment of Common and Reparameterized (meta-)GGA Density Functionals. *J. Chem. Theory Comput.* **2010**, *6* (1), 107−126.

(27) (a) Riplinger, C.; Neese, F. An efficient and near linear scaling pair natural orbital based local coupled cluster method. *J. Chem. Phys.* **2013**, *138* (3), 034106. (b) Riplinger, C.; Sandhoefer, B.; Hansen, A.; Neese, F. Natural triple excitations in local coupled cluster calculations with pair natural orbitals. *J. Chem. Phys.* **2013**, *139* (13), 134101.

(28) Hansen, A.; Bannwarth, C.; Grimme, S.; Petrović, P.; Werlé, C.; Djukic, J.-P. The Thermochemistry of London Dispersion-Driven Transition Metal Reactions: Getting the "Right Answer for the Right Reason". *ChemistryOpen* **2014**, *3* (5), 177−189.

(29) Hansen, A.; Neese, F.; Grimme, S. To be submitted for publication.

(30) Liakos, D. G.; Sparta, M.; Kesharwani, M. K.; Martin, J. M. L.; Neese, F. Exploring the Accuracy Limits of Local Pair Natural Orbital Coupled-Cluster Theory. *J. Chem. Theory Comput.* **2015**, *11* (4), 1525−1539.

(31) Mládek, A.; Banáš, P.; Jurečka, P.; Otyepka, M.; Zgarbová, M.; Šponer, J. Energies and 2′-Hydroxyl Group Orientations of RNA Backbone Conformations. Benchmark CCSD(T)/CBS Database, Electronic Analysis, and Assessment of DFT Methods and MD Simulations. *J. Chem. Theory Comput.* **2014**, *10* (1), 463−480.

(32) Sato, T.; Nakai, H. Density functional method including weak interactions: Dispersion coefficients based on the local response approximation. *J. Chem. Phys.* **2009**, *131* (22), 224104.

(33) Vydrov, O. A.; Van Voorhis, T. Nonlocal van der Waals density functional: The simpler the better. *J. Chem. Phys.* **2010**, *133* (24), 244103.

(34) Hujo, W.; Grimme, S. Performance of the van der Waals Density Functional VV10 and (hybrid)GGA Variants for Thermochemistry and Noncovalent Interactions. *J. Chem. Theory Comput.* **2011**, *7* (12), 3866−3871.

(35) Hujo, W.; Grimme, S. Performance of Non-Local and Atom-Pairwise Dispersion Corrections to DFT for Structural Parameters of Molecules with Noncovalent Interactions. *J. Chem. Theory Comput.* **2013**, *9* (1), 308−315.

(36) Zhao, Y.; Truhlar, D. G. The M06 suite of density functionals for main group thermochemistry, thermochemical kinetics, noncovalent interactions, excited states, and transition elements: two new functionals and systematic testing of four M06-class functionals and 12 other functionals. *Theor. Chem. Acc.* **2008**, *120* (1−3), 215−241.

(37) Johnson, E. R.; Becke, A. D.; Sherrill, C. D.; DiLabio, G. A. Oscillations in meta-generalized-gradient approximation potential energy surfaces for dispersion-bound complexes. *J. Chem. Phys.* **2009**, *131* (3), 034111.

(38) Grimme, S.; Goerigk, L.; Fink, R. F. Spin-component-scaled electron correlation methods. *Wiley Interdiscip. Rev.: Comput. Mol. Sci.* **2012**, *2* (6), 886−906.

DOI: 10.1021/acs.jctc.5b00515
J. Chem. Theory Comput. 2015, 11, 4972−4991

(39) Kong, L.; Bischoff, F. A.; Valeev, E. F. Explicitly Correlated R12/F12 Methods for Electronic Structure. *Chem. Rev.* **2012**, *112* (1), 75−107.
(40) Stewart, J. J. P. Optimization of parameters for semiempirical methods V: Modification of NDDO approximations and application to 70 elements. *J. Mol. Model.* **2007**, *13* (12), 1173−1213.
(41) (a) Gaus, M.; Cui, Q.; Elstner, M. DFTB3: Extension of the Self-Consistent-Charge Density-Functional Tight-Binding Method (SCC-DFTB). *J. Chem. Theory Comput.* **2011**, *7* (4), 931−948. (b) Brandenburg, J. G.; Grimme, S. Accurate Modeling of Organic Molecular Crystals by Dispersion-Corrected Density Functional Tight Binding (DFTB). *J. Phys. Chem. Lett.* **2014**, *5* (11), 1785−1789.
(42) Sure, R.; Grimme, S. Corrected small basis set Hartree−Fock method for large systems. *J. Comput. Chem.* **2013**, *34* (19), 1672−1685.
(43) (a) Cornell, W. D.; Cieplak, P.; Bayly, C. I.; Gould, I. R.; Merz, K. M.; Ferguson, D. M.; Spellmeyer, D. C.; Fox, T.; Caldwell, J. W.; Kollman, P. A. A 2nd Generation Force-Field for the Simulation of Proteins, Nucleic-Acids, and Organic-Molecules. *J. Am. Chem. Soc.* **1995**, *117* (19), 5179−5197. (b) Perez, A.; Marchan, I.; Svozil, D.; Sponer, J.; Cheatham, T. E.; Laughton, C. A.; Orozco, M. Refinenement of the AMBER force field for nucleic acids: Improving the description of alpha/gamma conformers. *Biophys. J.* **2007**, *92* (11), 3817−3829. (c) Zgarbova, M.; Otyepka, M.; Sponer, J.; Mladek, A.; Banas, P.; Cheatham, T. E.; Jurecka, P. Refinement of the Cornell et al. Nucleic Acids Force Field Based on Reference Quantum Chemical Calculations of Glycosidic Torsion Profiles. *J. Chem. Theory Comput.* **2011**, *7* (9), 2886−2902.
(44) Neese, F. The ORCA program system. *Wiley Interdiscip. Rev.: Comput. Mol. Sci.* **2012**, *2* (1), 73−78.
(45) Frisch, M. J.; Trucks, G. W.; Schlegel, H. B.; Scuseria, G. E.; Robb, M. A.; Cheeseman, J. R.; Scalmani, G.; Barone, V.; Mennucci, B.; Petersson, G. A.; Nakatsuji, H.; Caricato, M.; Li, X.; Hratchian, H. P.; Izmaylov, A. F.; Bloino, J.; Zheng, G.; Sonnenberg, J. L.; Hada, M.; Ehara, M.; Toyota, K.; Fukuda, R.; Hasegawa, J.; Ishida, M.; Nakajima, T.; Honda, Y.; Kitao, O.; Nakai, H.; Vreven, T.; Montgomery Jr., J. A.; Peralta, J. E.; Ogliaro, F.; Bearpark, M. J.; Heyd, J.; Brothers, E. N.; Kudin, K. N.; Staroverov, V. N.; Kobayashi, R.; Normand, J.; Raghavachari, K.; Rendell, A. P.; Burant, J. C.; Iyengar, S. S.; Tomasi, J.; Cossi, M.; Rega, N.; Millam, N. J.; Klene, M.; Knox, J. E.; Cross, J. B.; Bakken, V.; Adamo, C.; Jaramillo, J.; Gomperts, R.; Stratmann, R. E.; Yazyev, O.; Austin, A. J.; Cammi, R.; Pomelli, C.; Ochterski, J. W.; Martin, R. L.; Morokuma, K.; Zakrzewski, V. G.; Voth, G. A.; Salvador, P.; Dannenberg, J. J.; Dapprich, S.; Daniels, A. D.; Farkas, Ö.; Foresman, J. B.; Ortiz, J. V.; Cioslowski, J.; Fox, D. J. *Gaussian 09*; Gaussian, Inc.: Wallingford, CT, USA, 2009.
(46) Schmidt, M. W.; Baldridge, K. K.; Boatz, J. A.; Elbert, S. T.; Gordon, M. S.; Jensen, J. H.; Koseki, S.; Matsunaga, N.; Nguyen, K. A.; Su, S.; Windus, T. L.; Dupuis, M.; Montgomery, J. A. General atomic and molecular electronic structure system. *J. Comput. Chem.* **1993**, *14* (11), 1347−1363.
(47) Stewart, J. J. P. *MOPAC2012*; Stewart Computational Chemistry; Colorado Springs, CO, USA, 2012.
(48) Case, D. A.; Darden, T.; Cheatham, T. E., III; Simmerling, C. L.; Wang, J.; Duke, R. E.; Luo, R.; Walker, R. C.; Zhang, W.; Merz, K. M.; Roberts, B.; Hayik, S.; Roitberg, A.; Seabra, G.; Swails, J.; Götz, A. W.; Kolossváry, I.; Wong, K. F.; Paesani, F.; Vanicek, J.; Wolf, R. M.; Liu, J.; Wu, X.; Brozell, S. R.; Steinbrecher, T.; Gohlke, H.; Cai, Q.; Ye, X.; Wang, J.; Hsieh, M.-J.; Cui, G.; Roe, D. R.; Mathews, D. H.; Seetin, M. G.; R. Salomon-Ferrer, Sagui, C.; Babin, V.; Luchko, T.; Gusarov, S.; Kovalenko, A.; Kollman, P. A. *Amber12*; University of California: San Francisco, CA, 2012.
(49) Aradi, B.; Hourahine, B.; Frauenheim, T. DFTB+, a sparse matrix-based implementation of the DFTB method. *J. Phys. Chem. A* **2007**, *111* (26), 5678−5684.
(50) (a) Ahlrichs, R.; Bar, M.; Haser, M.; Horn, H.; Kolmel, C. Electronic-Structure Calculations on Workstation Computers—The Program System Turbomole. *Chem. Phys. Lett.* **1989**, *162* (3), 165−169. (b) *TURBOMOLE V 6.3*, a development of University of Karlsruhe and Forschungszentrum Karlsruhe GmbH, 1989−2007 (since 2007, TURBOMOLE GmbH, 2013.
(51) Peverati, R.; Truhlar, D. G. M11-L: A Local Density Functional That Provides Improved Accuracy for Electronic Structure Calculations in Chemistry and Physics. *J. Phys. Chem. Lett.* **2012**, *3* (1), 117−124.
(52) Peverati, R.; Truhlar, D. G. Improving the Accuracy of Hybrid Meta-GGA Density Functionals by Range Separation. *J. Phys. Chem. Lett.* **2011**, *2* (21), 2810−2817.
(53) Peverati, R.; Truhlar, D. G. Communication: A global hybrid generalized gradient approximation to the exchange-correlation functional that satisfies the second-order density-gradient constraint and has broad applicability in chemistry. *J. Chem. Phys.* **2011**, *135* (19), 191102.
(54) Dapprich, S.; Komáromi, I.; Byun, K. S.; Morokuma, K.; Frisch, M. J. A new ONIOM implementation in Gaussian98. Part I. The calculation of energies, gradients, vibrational frequencies and electric field derivatives. *J. Mol. Struct.: THEOCHEM* **1999**, *461−462*, 1−21.
(55) Weigend, F. Accurate Coulomb-fitting basis sets for H to Rn. *Phys. Chem. Chem. Phys.* **2006**, *8* (9), 1057−1065.
(56) Schuchardt, K. L.; Didier, B. T.; Elsethagen, T.; Sun, L. S.; Gurumoorthi, V.; Chase, J.; Li, J.; Windus, T. L. Basis set exchange: A community database for computational sciences. *J. Chem. Inf. Model.* **2007**, *47* (3), 1045−1052.
(57) Tao, J. M.; Perdew, J. P.; Staroverov, V. N.; Scuseria, G. E. Climbing the density functional ladder: Nonempirical meta-generalized gradient approximation designed for molecules and solids. *Phys. Rev. Lett.* **2003**, *91* (14), 146401.
(58) Lebedev, V. I.; Laikov, D. N. Quadrature formula for the sphere of 131st algebraic order of accuracy. *Dokl. Akad. Nauk* **1999**, *366* (6), 741−745.
(59) Stewart, J. P. Optimization of parameters for semiempirical methods. VI: More modifications to the NDDO approximations and re-optimization of parameters. *J. Mol. Model.* **2013**, *19* (1), 1−32.
(60) Kromann, J. C.; Christensen, A. S.; Steinmann, C.; Korth, M.; Jensen, J. H. A third-generation dispersion and third-generation hydrogen bonding corrected PM6 method: PM6-D3H+. *PeerJ* **2014**, *2*, e449.
(61) Grimme, S.; Antony, J.; Ehrlich, S.; Krieg, H. A consistent and accurate *ab initio* parametrization of density functional dispersion correction (DFT-D) for the 94 elements H−Pu. *J. Chem. Phys.* **2010**, *132* (15), 154104.
(62) Izsak, R.; Neese, F. An overlap fitted chain of spheres exchange method. *J. Chem. Phys.* **2011**, *135* (14), 144105.
(63) Kruse, H.; Grimme, S. A geometrical correction for the inter- and intra-molecular basis set superposition error in Hartree-Fock and density functional theory calculations for large systems. *J. Chem. Phys.* **2012**, *136* (15), 154101.10.1063/1.3700154
(64) Rappoport, D.; Furche, F. Property-optimized Gaussian basis sets for molecular response calculations. *J. Chem. Phys.* **2010**, *133* (13), 134105.
(65) Weigend, F.; Kohn, A.; Hattig, C. Efficient use of the correlation consistent basis sets in resolution of the identity MP2 calculations. *J. Chem. Phys.* **2002**, *116* (8), 3175−3183.
(66) Klamt, A.; Schürmann, G. Cosmo—A New Approach to Dielectric Screening in Solvents with Explicit Expressions for the Screening Energy and Its Gradient. *J. Chem. Soc., Perkin Trans. 2* **1993**, No. 5, 799−805.
(67) Grimme, S.; Ehrlich, S.; Goerigk, L. Effect of the Damping Function in Dispersion Corrected Density Functional Theory. *J. Comput. Chem.* **2011**, *32* (7), 1456−1465.
(68) Richardson, D. C. *Suitename, v. 0.3.070628*; http://kinemage.biochem.duke.edu/software/.
(69) Humphrey, W.; Dalke, A.; Schulten, K. VMD: Visual molecular dynamics. *J. Mol. Graphics* **1996**, *14* (1), 33−38.
(70) Hobza, P.; Sponer, J. Significant structural deformation of nucleic acid bases in stacked base pairs: An *ab initio* study beyond Hartree−Fock. *Chem. Phys. Lett.* **1998**, *288* (1), 7−14.

DOI: 10.1021/acs.jctc.5b00515
J. Chem. Theory Comput. 2015, 11, 4972−4991

(71) Hesselmann, A.; Korona, T. Intermolecular symmetry-adapted perturbation theory study of large organic complexes. *J. Chem. Phys.* **2014**, *141* (9), 094107.
(72) Goerigk, L.; Grimme, S. Efficient and Accurate Double-Hybrid-Meta-GGA Density Functionals-Evaluation with the Extended GMTKN30 Database for General Main Group Thermochemistry, Kinetics, and Noncovalent Interactions. *J. Chem. Theory Comput.* **2011**, *7* (2), 291−309.
(73) Karton, A.; Martin, J. L. Comment on: "Estimating the Hartree−Fock limit from finite basis set calculations". *Theor. Chem. Acc.* **2006**, *115* (4), 330−333.
(74) Halkier, A.; Helgaker, T.; Jorgensen, P.; Klopper, W.; Koch, H.; Olsen, J.; Wilson, A. K. Basis-set convergence in correlated calculations on Ne, N_2, and H_2O. *Chem. Phys. Lett.* **1998**, *286* (3−4), 243−252.
(75) Truhlar, D. G. Basis-set extrapolation. *Chem. Phys. Lett.* **1998**, *294* (1−3), 45−48.
(76) Neese, F.; Valeev, E. F. Revisiting the Atomic Natural Orbital Approach for Basis Sets: Robust Systematic Basis Sets for Explicitly Correlated and Conventional Correlated *Ab Initio* Methods? *J. Chem. Theory Comput.* **2011**, *7* (1), 33−43.
(77) Csaszar, A. G.; Allen, W. D.; Schaefer, H. F. In pursuit of the *Ab Initio* limit for conformational energy prototypes. *J. Chem. Phys.* **1998**, *108* (23), 9751−9764.
(78) Hobza, P.; Sponer, J. Toward true DNA base-stacking energies: MP2, CCSD(T), and complete basis set calculations. *J. Am. Chem. Soc.* **2002**, *124* (39), 11802−11808.
(79) Lilley, D. M. J. The K-turn motif in riboswitches and other RNA species. *Biochim. Biophys. Acta, Gene Regul. Mech.* **2014**, *1839* (10), 995−1004.
(80) Ruscic, B. Uncertainty Quantification in Thermochemistry, Benchmarking Electronic Structure Computations, and Active Thermochemical Tables. *Int. J. Quantum Chem.* **2014**, *114* (17), 1097−1101.
(81) Perdew, J. P.; Schmidt, K. Jacob's ladder of density functional approximations for the exchange-correlation energy. *AIP Conf. Proc.* **2000**, *577* (1), 1−20.
(82) Schwabe, T.; Grimme, S. Double-hybrid density functionals with long-range dispersion corrections: Higher accuracy and extended applicability. *Phys. Chem. Chem. Phys.* **2007**, *9* (26), 3397−3406.
(83) Karton, A.; Tarnopolsky, A.; Lamère, J.-F.; Schatz, G. C.; Martin, J. M. L. Highly Accurate First-Principles Benchmark Data Sets for the Parametrization and Validation of Density Functional and Other Approximate Methods. Derivation of a Robust, Generally Applicable, Double-Hybrid Functional for Thermochemistry and Thermochemical Kinetics. *J. Phys. Chem. A* **2008**, *112* (50), 12868−12886.
(84) Kozuch, S.; Gruzman, D.; Martin, J. M. L. DSD-BLYP: A General Purpose Double Hybrid Density Functional Including Spin Component Scaling and Dispersion Correction. *J. Phys. Chem. C* **2010**, *114* (48), 20801−20808.
(85) Zhao, Y.; Truhlar, D. G. Design of density functionals that are broadly accurate for thermochemistry, thermochemical kinetics, and nonbonded interactions. *J. Phys. Chem. A* **2005**, *109* (25), 5656−5667.
(86) (a) Lee, D.; Furche, F.; Burke, K. Accuracy of Electron Affinities of Atoms in Approximate Density Functional Theory. *J. Phys. Chem. Lett.* **2010**, *1* (14), 2124−2129. (b) Kim, M. C.; Sim, E.; Burke, K. Communication: Avoiding unbound anions in density functional calculations. *J. Chem. Phys.* **2011**, *134* (17).17110310.1063/1.3590364
(87) Ciofini, I.; Adamo, C.; Chermette, H. Self-interaction error in density functional theory: A mean-field correction for molecules and large systems. *Chem. Phys.* **2005**, *309* (1), 67−76.
(88) (a) DiStasio, R. A., Jr.; Gobre, W. V.; Tkatchenko, A. Many-body van der Waals interactions in molecules and condensed matter. *J. Phys.: Condens. Matter* **2014**, *26* (21), 213202. (b) Risthaus, T.; Grimme, S. Benchmarking of London Dispersion-Accounting Density Functional Theory Methods on Very Large Molecular Complexes. *J. Chem. Theory Comput.* **2013**, *9* (3), 1580−1591.
(89) (a) Zgarbova, M.; Luque, F. J.; Sponer, J.; Cheatham, T. E.; Otyepka, M.; Jurecka, P. Toward Improved Description of DNA Backbone: Revisiting Epsilon and Zeta Torsion Force Field Parameters. *J. Chem. Theory Comput.* **2013**, *9* (5), 2339−2354. (b) Krepl, M.; Zgarbova, M.; Stadlbauer, P.; Otyepka, M.; Banas, P.; Koca, J.; Cheatham, T. E.; Jurecka, P.; Sponer, J. Reference Simulations of Noncanonical Nucleic Acids with Different χ Variants of the AMBER Force Field: Quadruplex DNA, Quadruplex RNA, and Z-DNA. *J. Chem. Theory Comput.* **2012**, *8* (7), 2506−2520.
(90) (a) Hawkins, G. D.; Cramer, C. J.; Truhlar, D. G. Pairwise Solute Descreening of Solute Charges from a Dielectric Medium. *Chem. Phys. Lett.* **1995**, *246* (1−2), 122−129. (b) Tsui, V.; Case, D. A. Theory and applications of the generalized Born solvation model in macromolecular Simulations. *Biopolymers* **2000**, *56* (4), 275−291.
(91) Yildirim, I.; Stern, H. A.; Kennedy, S. D.; Tubbs, J. D.; Turner, D. H. Reparameterization of RNA χ Torsion Parameters for the AMBER Force Field and Comparison to NMR Spectra for Cytidine and Uridine. *J. Chem. Theory Comput.* **2010**, *6* (5), 1520−1531.
(92) Chen, A. A.; Garcia, A. E. High-resolution reversible folding of hyperstable RNA tetraloops using molecular dynamics simulations. *Proc. Natl. Acad. Sci. U. S. A.* **2013**, *110* (42), 16820−5.
(93) Denning, E. J.; Priyakumar, U. D.; Nilsson, L.; Mackerell, A. D. Impact of 2′-hydroxyl sampling on the conformational properties of RNA: Update of the CHARMM all-atom additive force field for RNA. *J. Comput. Chem.* **2011**, *32* (9), 1929−1943.
(94) Korth, M. Error estimates for (semi-)empirical dispersion terms and large biomacromolecules. *Org. Biomol. Chem.* **2013**, *11* (38), 6515−6519.
(95) Brandenburg, J. G.; Hochheim, M.; Bredow, T.; Grimme, S. Low-Cost Quantum Chemical Methods for Noncovalent Interactions. *J. Phys. Chem. Lett.* **2014**, *5* (24), 4275−4284.
(96) Goerigk, L.; Karton, A.; Martin, J. M. L.; Radom, L. Accurate quantum chemical energies for tetrapeptide conformations: Why MP2 data with an insufficient basis set should be handled with caution. *Phys. Chem. Chem. Phys.* **2013**, *15* (19), 7028−7031.
(97) Liakos, D. G.; Izsak, R.; Valeev, E. F.; Neese, F. What is the most efficient way to reach the canonical MP2 basis set limit? *Mol. Phys.* **2013**, *111* (16−17), 2653−2662.
(98) Krasovska, M. V.; Sefcikova, J.; Reblova, K.; Schneider, B.; Walter, N. G.; Sponer, J. Cations and hydration in catalytic RNA: Molecular dynamics of the hepatitis delta virus ribozyme. *Biophys. J.* **2006**, *91* (2), 626−638.
(99) (a) Delvalle, F. J. O.; Tomasi, J. Electron Correlation and Solvation Effects. 1. Basic Formulation and Preliminary Attempt To Include the Electron Correlation in the Quantum-Mechanical Polarizable Continuum Model So as To Study Solvation Phenomena. *Chem. Phys.* **1991**, *150* (2), 139−150. (b) Angyan, J. G. Choosing between Alternative MP2 Algorithms in the Self-Consistent Reaction Field-Theory of Solvent Effects. *Chem. Phys. Lett.* **1995**, *241* (1−2), 51−56.
(100) Savelyev, A.; MacKerell, A. D. All-Atom Polarizable Force Field for DNA Based on the Classical Drude Oscillator Model. *J. Comput. Chem.* **2014**, *35* (16), 1219−1239.

DOI: 10.1021/acs.jctc.5b00515
J. Chem. Theory Comput. 2015, 11, 4972−4991